APTAMER TARGETED DRUG DELIVERY AND PROGRESS TOWARDS NOVEL BIOMARKER IDENTIFICATION IN HEPATOCELLULAR CARCINOMA CELLS

by

Elizabeth Irene McIvor, B.S.

A thesis submitted to the Graduate Council of
Texas State University in partial fulfillment
of the requirements for the degree of
Master of Science
with a Major in Biochemistry
August 2017

Committee Members:

Kevin Lewis, Chair

Shannon Weigum, Co-Chair

Liqin Du

FAIR USE AND AUTHOR'S PERMISSION STATEMENT

Fair Use

Duplication Permission

DEDICATION

This work is dedicated to my father, James G. McIvor, who passed away in 2006 from complications of pancreatic cancer. He was one of the most unique men I have ever known, and his dedication to his family was unparalleled. My decision to return to university as a graduate student after working in academia in many ways reflects his decision to pursue completion of an engineering degree at a similar point in his life. Among so many other things, you taught me what's *right*, and what's *important*, and I've since learned that those two things are sometimes not easily reconciled. I love you, I miss you, and I hope you are proud of me.

To my mother, MaryAnn: there is no way to express my thanks to you in a written dedication. Your love and support have carried me through the hardest of unbelievably hard times. Wherever you are is my home, and you will always have a home with me.

I have innumerable friends, colleagues, and loved ones to thank for their support and guidance over the last couple of years. DAL, I love you and I can't wait to change the world with you. ECP, your kindness and grace are beyond measure and expectation, I'll be forever thankful for you. BA, your support and advice have been invaluable and I look forward to the day that we can work together again. TYF, the world took you too soon, and I will never forget your unwavering friendship and encouragement. CAM and JMC, together we were the original dynamic trio; you two have made me so proud and I know the future holds great things for both of you. VKH and JKT, so many thanks to both of you for the duration, and especially in the home stretch. Love to you all.

ACKNOWLEDGEMENTS

First and foremost, I would like to express my deep thanks and gratitude to Dr. Shannon Weigum for taking me on as a student. In accepting a student from a different department, she took on unique challenges and responsibilities, not all of which were apparent from the beginning. Her patience, understanding, advice, professionalism, and humanity were all instrumental to my success in completing this work. She is a wonderful mentor and a great force for good in science.

I'd like to extend an equal measure of these sentiments to Dr. Kevin Lewis, as my anchor in the department of Chemistry and Biochemistry. Without his help, advice, kindness and compassion, none of this would have been possible.

I would like to thank Dr. Tania Betancourt and Christopher Munoz from her lab for their gracious and kind support, lots of shared time and supplies, and exceptional collaborative efforts. Additional thanks to Dr. Liqin Du for serving on my committee, taking time to meet with me, and generous gifts of supplies.

Finally, I'd like to acknowledge all of my fellow Weigum Lab members, past and present. Wonderful lab-mates are not universal, but all of them have been truly exceptional and will continue to be great contributors to science.

This work was supported by funding from the Texas State University Research Enhancement Program.

TABLE OF CONTENTS

Page

LIST OF TABLES

Table **Page**

LIST OF FIGURES

Figure **Page**

LIST OF ABBREVIATIONS

Abbreviation	Description
DPBS	Dulbecco's modified phosphate buffered saline
DMSO	Dimethyl sulfoxide
DTT	Dithiothreitol
ECL	Enhanced chemiluminescent substrate
EGF	Epidermal growth factor
HRP	Horseradish peroxidase
K_d	Dissociation constant
mQ H_2O	Millipore purified water
MTT	Methylthiazolyldiphenyl-tetrazolium bromide
NFDM	Non-fat dry milk
PCR	Polymerase chain reaction
PES	Polyethersulfone
PTFE	Polytetrafluoroethylene
PVDF	Polyvinylidene difluoride
RT	Room temperature
TBS	Tris buffered saline
TEG	Tetraethyleneglycol

1. INTRODUCTION

1.1. Liver Cancer

Liver cancer is a highly fatal disease. Prognosis is extremely poor, with a mortal outcome in 95% of diagnosed cases worldwide.[1–3] In contrast to declining trends for the 4 major types of cancer, deaths from liver cancer in the United States have increased by nearly 3% each year since 2000.[1,4] Less developed countries bear a higher burden of overall incidence, but the mortality to incidence ratio is similar regardless of geography (Figure 1). Primary risk factors for liver cancer include chronic viral hepatitis (hepatitis B and hepatitis C), alcohol abuse, obesity, diabetes, exposure to aflatoxin, and tobacco use.[4,5]

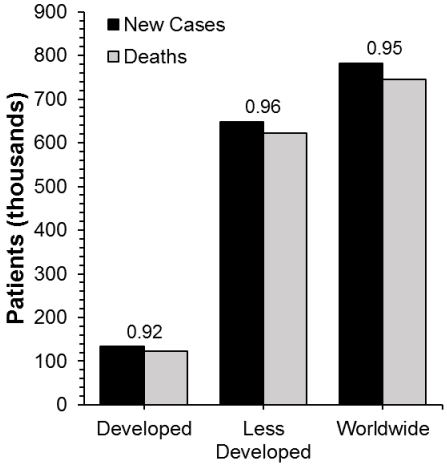

Figure 1. Estimated number of new cases and deaths from liver cancer for 2012. GLOBOCAN estimates of liver cancer trends for 2012.[3] Ratios of mortality to incidence are shown above each category.

Hepatocellular carcinoma (HCC) comprises an estimated 75-90% of all liver cancer diagnoses.[4,6] In the United States, patients that exhibit high risk of developing HCC are routinely referred for disease surveillance, where their condition is frequently

monitored by various imaging modalities and assessment of known biomarkers.[5,7] However, surveillance has not been shown to reduce mortality from HCC.[4] Over 90% of HCC cases present concomitantly with cirrhosis (significant scarring of liver tissue) and thus underlying hepatic dysfunction.[2] This causes significant complications in clinical management of these patients, as cancer treatment must be carefully selected, and balanced against the possibility of further damage to remaining healthy liver tissue.[2,5,8]

Diagnosing HCC in its earliest stages when the best treatments are feasible has proven problematic. Clinical symptoms of HCC typically do not appear until late stage disease.[9] Even with surveillance, catching HCC early is difficult. Diagnostic imaging indicating small HCC tumors is unreliable, and biopsies are risky to the patient (due to the risk of "seeding" - mechanically spreading malignant cells), and potentially uninformative due to lack of consensus among pathologists regarding tumor stage grading.[5,8] Serological testing presents further obstacles, as circulating biomarkers indicative of HCC have limited utility as they can have low specificity, low sensitivity, or provide false negatives or positives.[9] For these reasons, it is unsurprising that HCC is typically diagnosed at stages when treatment options are severely limited.

Treatments for early stage HCC that are considered to be curative include: liver transplantation, resection (surgical removal of the cancer or a portion of the liver), and ablation (physical or chemical destruction of tumor tissue).[2] Although liver transplants offer the best outcomes, they are limited by the number of donors, and the characteristics of underlying liver disease in each patient.[7] Even with liver transplantation, tumor recurrence can affect 15-25% of these patients.[5] Resection and ablation offer increases in survival time, but cancer recurrence is a major problem after these procedures, affecting

around 70% of patients in 4 to 5 years.[2,5,7] The 5-year survival rate is a common metric for tracking outcomes in cancer. However, this metric can be misleading given the gap between 5-year survival (Figure 2) and the overall mortality rate (Figure 1).

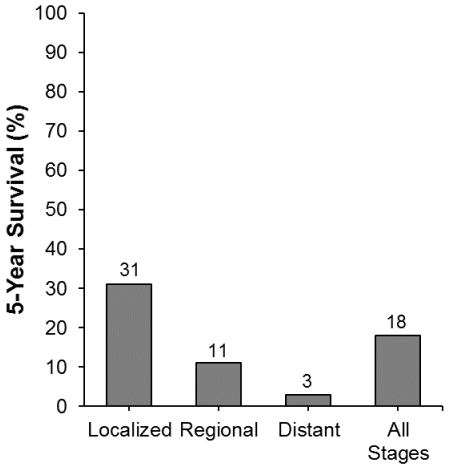

Figure 2. Overall 5-year survival rates for liver cancer by stage at diagnosis in the US. Survival rates from 2006-2012[4] in percent of diagnosed cases. Values are listed above bars.

No potentially curative options currently exist for intermediate or late stage HCC, and treatments are geared toward increasing patient survival time and providing palliative care.[5] For treatment of intermediate HCC, transarterial chemoembolization (TACE) is a method employed to obstruct blood flow to the area of the tumor, aimed at reducing the time to disease progression. A single chemotherapeutic, sorafenib, is FDA approved for treatment of advanced HCC.[10] Sorafenib is a small molecule drug that inhibits activation of certain growth factors that are overexpressed in cancer. However, sorafenib only offers a short survival benefit (a few months), can cause significant adverse side effects, and has not demonstrated improved quality of life in patients.[10,11] Excluding the very limited use and utility of sorafenib, no systemic chemotherapeutics have proven effective for treating

HCC, and are not recommended even as a last resort.[2]

The grim realities of HCC prognosis, difficulties with early diagnosis, and the paucity of effective treatments point to a critical need for the development of novel therapeutic modalities for this fatal disease.

1.2. Tumor Characteristics and Current Chemotherapeutics

The rapid growth of cancer cells versus normal cells was the initial point of exploit for early chemotherapeutics, and remains a major consideration in the development of new approaches to cancer therapy. Tumor growth demands significant nutrients from the bloodstream, and the formation of new blood vessels, called angiogenesis, proceeds rapidly in cancer tissue to meet these needs.[12–14] The resulting vasculature is poorly organized and improperly structured compared to that of normal tissue.[12] The cells comprising tumor capillaries are not tightly joined, leading to gaps 100 nm to microns in size called fenestrations.[13,14] Additionally, increased fibrosity in the extracellular matrix of the tumor microenvironment combined with poor lymphatic drainage causes high interstitial pressure within tumors.[14] Figure 3 illustrates these physiological hallmarks.[15]

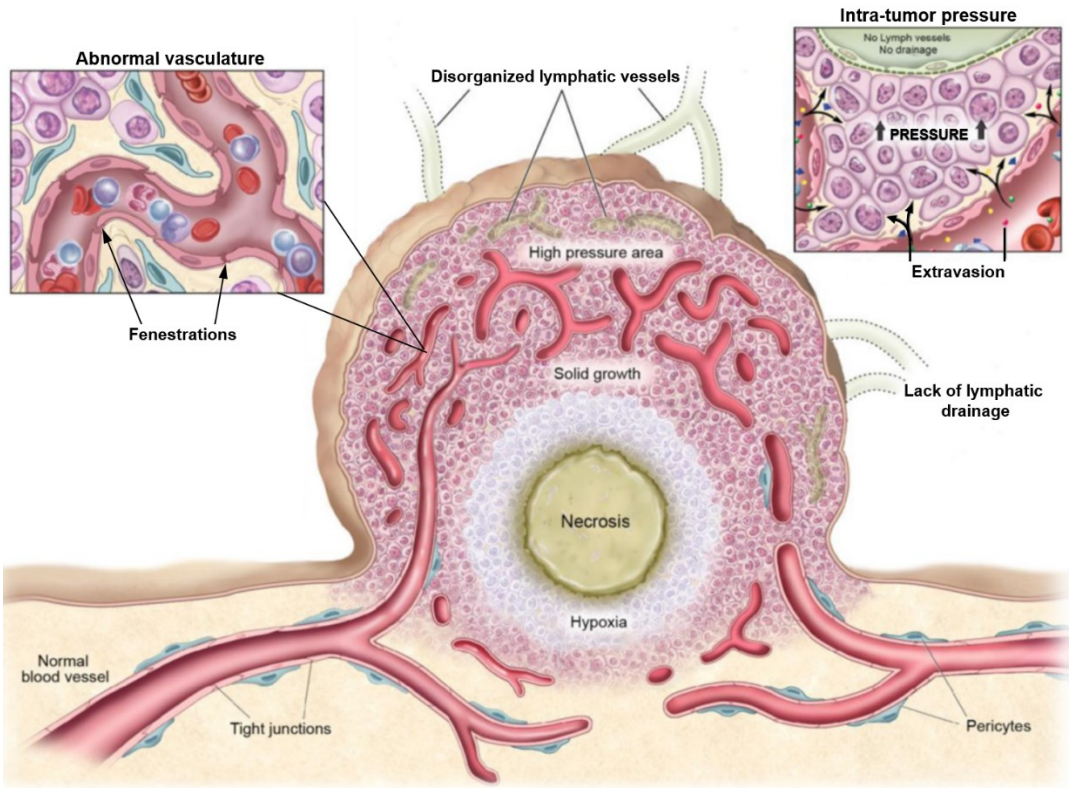

Figure 3. Illustration of tumor physiology. Disordered blood and lymphatic vessels lead to a combination of unique characteristics associated with solid tumors. Small molecules in circulation are subject to efflux from the internal tumor environment due to high interstitial pressure, while larger circulating particles can extravasate through fenestrations and become trapped. Published image re-used under open access policy.[15]

Small molecules are easily forced out of this environment, which is a major problem associated with traditional chemotherapeutics as delivery of optimal drug concentration to the interior of tumors is not easily achieved.[12,15] Systemic administration of therapeutics must thus be balanced to achieve anti-tumor efficacy while avoiding toxicity in normal tissue. This creates a barrier to delivering drugs at concentrations best suited to killing cancer without killing the patient. The development of novel approaches to drug delivery that can both harness the cytotoxic efficacy of traditional chemotherapeutics and minimize unwanted off-target effects is currently an area of significant research efforts.[13]

1.3. Nanomedicine and Drug Delivery

The term nanomedicine refers to the interface of nanotechnology and the treatment of disease. Nanoscale structures ranging in size from 1 nanometer to 1,000 nanometers have unique physical properties and consequently unique physiological properties when introduced into cells or whole organisms.[14,16,17] The potential clinical applications of nanomaterials are vast, and research into nanotherapeutics has increased very rapidly in recent years. As of 2016, 51 drugs qualifying as nanomedicines have been approved by the FDA, with an additional 77 currently in clinical trials.[17] The use of nanomedicine in the treatment of cancer has significant appeal, as the unique properties associated with nanomaterials are particularly well suited to address the issues associated with cancer tissue and traditional treatments outlined above.

Nanoparticles (NPs), which are defined by a size of ~100 nm and a spherical shape, may consist of virtually any material including metal, carbon, polymers, and proteins, thus providing for massive flexibility in design and functionality.[14,16–19] Polymeric NPs can be engineered from a variety of biodegradable polymers that break down into non-toxic monomers that are eliminable *in vivo*.[14] Small molecule drugs, therapeutic peptides, or nucleic acids can be encapsulated into polymeric NPs, which afford protection from rapid metabolic clearance and degradation.[20] The characteristic vascular architecture of tumors described in section 1.2 and illustrated in Figure 3 result in a phenomenon known as the enhanced permeability and retention (EPR) effect: particles that are too large to enter most normal vasculature can penetrate the interstitial space of tumors via fenestrations, but are then retained due to the reduction in lymphatic

clearance.[13,14,21] Passive targeting of cancer tissue can thus be achieved with NPs, where extravasation and accumulation in the tumor microenvironment allows for local and sustained release of drug payload, increasing the effective dose to the tumor while limiting exposure to healthy tissue.[21] Controlled drug release from polymeric NPs can be tuned based on polymer composition and NP preparation.[20,22] This can significantly improve the pharmacokinetic and bio-distribution profiles of existing drugs.[20] In addition to passive targeting via the EPR effect, the surface of NPs can be decorated with affinity ligands that promote localization to cancer tissues that harbor their cognate targets.[13,20] Utilizing cell surface biomarkers is a significant area of interest in this regard. The identification biomarkers that may be present in low abundance but are nevertheless unique to a particular cancer type, such as HCC, will enable more comprehensive studies of actively targeted drug nanocarriers.

1.4. Aptamers

Aptamers are high affinity ligands comprised of single-stranded nucleic acids or nucleic acid analogs that fold into specific secondary structures.[23–25] Like antibodies, aptamers bind to their cognate targets with high affinity and specificity, with reported K_d values from the nanomolar to picomolar range.[26] Aptamers can recognize an impressive array of targets including ions, small molecules, biomolecules, and whole cells.[27–29] In contrast to antibodies, which are expensive, particularly labile, and frequently immunogenic, aptamers are stable over a wide range of environmental conditions, are non-immunogenic, and can be produced rapidly in relatively high quantity at lower overall cost.[29] Synthetic oligonucleotides are made with the phosphoramidite method,

which allows for facile incorporation of functional moieties into aptamers by addition of pre-modified nucleotides during synthesis.[30,31] Common functional modifications include fluorescent reporters, affinity tags, and chemical groups that enable post-synthesis attachment to solid surfaces or other molecules. Importantly, inclusion of these groups at the 5′ and/or 3′ ends of aptamers do not disrupt their secondary structure.[26] The functionalization and immobilization of antibodies is significantly more difficult. Depending on the type of conjugation chemistry, non-site-specific attachment can occur at undesired locations on the protein leading to disruption of antibody-antigen recognition and decreasing sensitivity.[32] The beneficial properties of aptamers impart many potential advantages to research, diagnostic, and therapeutic applications where antibodies have proven to be problematic.[33,34]

Aptamer-target binding occurs via shape-based recognition which relies on a variety of non-covalent interactions such as hydrogen bonding, electrostatic attraction, van der Waals forces, and hydrophobic interactions.[35,36] Both formation of nucleic acid secondary and thus aptamer-target interaction can depend on ionic strength and pH of the environment. It has been demonstrated that the presence of divalent cations, particularly calcium and magnesium ions, can be critical to the stability of some aptamer-target complexes.[35] Moreover, magnesium mediates the complexation of water molecules during intermolecular interactions between DNA and proteins, and shields the negative charge associated with the phosphate backbone, preventing electrostatic repulsion of aptamers from cell surface targets.[30,37,38] Thus, the ionic composition of the environment in which aptamers were generated should be taken into consideration when developing novel biosensor or therapeutic platforms that include aptamers as targeting moieties.

1.5. Cell-SELEX

Aptamers are generated by systematic evolution of ligands by exponential enrichment (SELEX), in which a large library of oligonucleotides containing random sequences is incubated with the desired target substrate. Sequences that do not bind to the target are discarded by washing, and bound sequences are then purified and amplified with PCR. Subsequent repeated steps of incubation, washing, and PCR ultimately leads to enrichment for aptamers that have high affinity for the target substrate.[23,24] An adaptation of this method, called cell-SELEX (Figure 4), uses whole live cells as the positive selection target, enabling the generation of aptamers that recognize various types of proteins (Figure 5) present on the surface of cells.[28,39,40]

Cell-SELEX allows for the evolution of aptamers that recognize only specific cells. This is achieved with the addition of a counter-selection step (negative selection, Figure 4) to the SELEX procedure. The pool of oligonucleotides purified during the positive selection step is incubated with the undesired cell type and bound sequences are discarded from the library pool.[40–42] This critical step ensures that each cycle of enrichment only selects for sequences that exhibit affinity for the target cells.

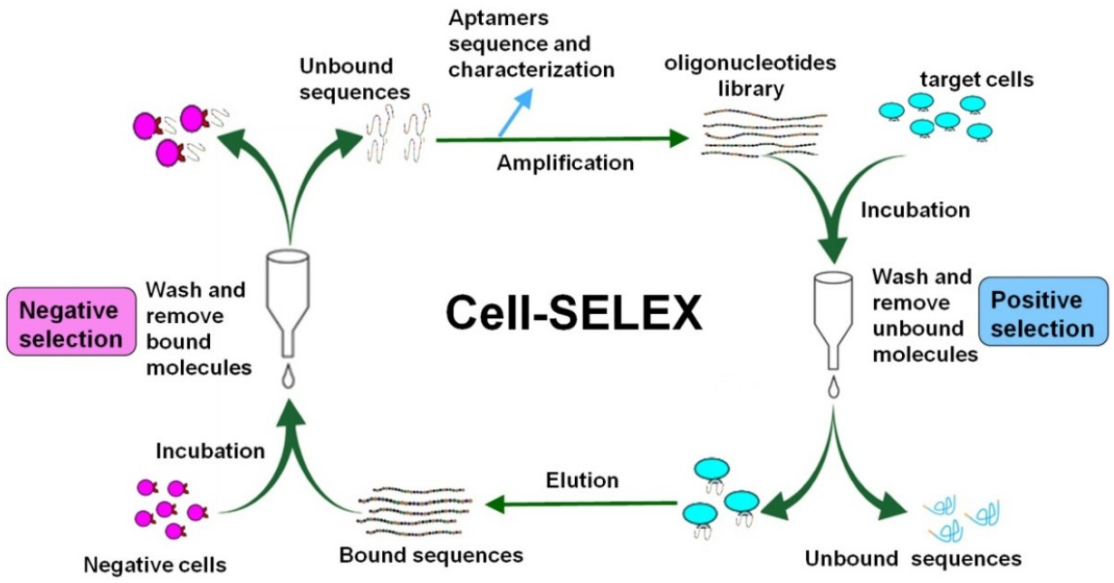

Figure 4. Schematic of cell-SELEX.[41] Published image re-used under open access policy.

A particularly useful application of cell-SELEX is creation of cancer-specific aptamers that do not bind to the parental cell type (e.g., normal tissue) as the composition of proteins on the surface of cancer cells is different from that of normal cells.[28,43,44] These may be any of a variety of types of proteins that associate with the cytosolic membrane, as long as part of the protein is external to the cell. Figure 5 illustrates the types, locations, and relative sizes of proteins associated with the cell membrane that may be targets of aptamers produced from cell-SELEX.

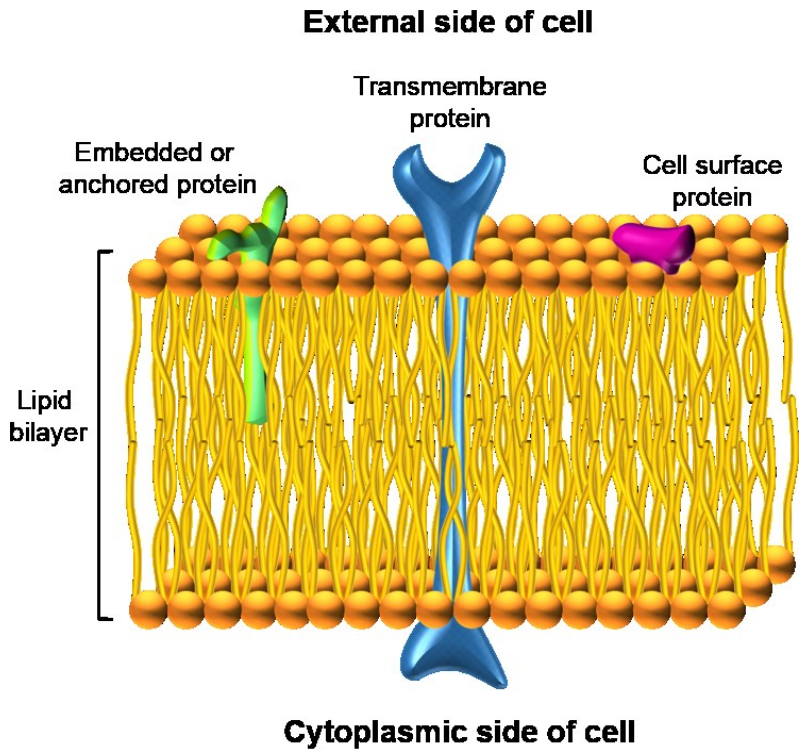

Figure 5. Depiction of proteins present at the surface of cells. Types of proteins that are present, in whole or part, on the external side of the cell membrane. Green: protein that is intrinsic to the cell membrane and may be either embedded in the lipid bilayer, or covalently anchored to it. Blue: transmembrane protein that is integral to the cell membrane, spans the lipid bilayer, and contains domains on both the extracellular and cytoplasmic sides of the cell. Pink: protein extrinsic to the cell membrane, but associated with the surface of the cell. The relative size of each protein depicted reflects the differences in molecular weights between the different types of proteins. Illustration is not explicitly drawn to scale.

Aptamers generated with this technique have been investigated for development of diagnostics, therapeutics, and novel biomarker identification.[28,43] Although cell-SELEX is a powerful tool to discover aptamers for cancer research, because the aptamers' targets are unknown at the time of development, identifying them requires additional research that can be difficult and labor intensive.[45]

1.6. HCC Specific Aptamer TLS11a

In 2008, the Tan group used cell-SELEX to identify a group of DNA aptamers

that recognized HCC cells but not normal hepatocytes.[46] In their study, BNL 1ME A.7R.1 (MEAR) cells, an HCC model cell line derived from chemically transformed mouse hepatocytes, was used for positive selection, and the parental normal mouse hepatocyte cell line BNL CL.2 (CL.2; referred to by Shangguan *et al*. and elsewhere as BNL) was used for counter selection.[46] Of the aptamers identified, TLS11a exhibited the highest affinity for the target cell type as determined by flow cytometry, with a reported K_d value of 4.51 ± 0.39 nM.[46]

Since the initial report of TLS11a, a number of studies have used this aptamer to investigate a variety of biosensor and drug delivery platforms.[47–57] Several of these reports demonstrated that TLS11a also recognizes human HCC cell lines but not normal human liver cells or other cancer cell lines; authors' results are summarized in Table 1.

Table 1. Cell lines previously tested for recognition by TLS11a. Positive or negative detection is listed as reported by study authors.

Cell Line	Cell Type	Species	TLS11a Recognition	References
MEAR	HCC (transformed hepatocyte)	Mouse	Yes	46,48,50,53
HepG2	HCC	Human	Yes	49,51,52,54–57
LH86	HCC	Human	Yes	47
CL.2	Normal hepatocyte	Mouse	No	46
Hu1229	Normal liver cells	Human	No	47
L02	Immortalized hepatocyte	Human	No	51,52,54,55,57
PC3	Prostate cancer	Human	No	49
MCF-7	Breast cancer	Human	No	49,51,52
HeLa	Cervical cancer	Human	No	50,54
293T	Embryonic kidney	Human	No	51
H9c2	Cardiomyoblast	Rat	No	52

This body of work lends strong support to the specificity of TLS11a towards HCC, and its potential utility for use in diagnostic and therapeutic applications. However, to date, no studies have been published that definitively identify the cellular target of TLS11a. Filling this gap in current knowledge is of critical importance, as it would elucidate a new biomarker for HCC and firmly qualify TLS11a as a viable tool for continued research.

1.7. Purification and Identification of Cell-SELEX Targets

The methods required for identification of cell-SELEX targets include affinity purification with ligand-modified aptamer, silver or colloidal staining of SDS-PAGE gels, mass spectrometry, knock-down and/or overexpression of putative targets, western blotting, fluorescence microscopy, and immunohistochemistry (IHC).[45,58–63] These methods can be labor intensive, time consuming, and expensive. One report describes the use of stable-isotope labeling by amino acids in cell culture (SILAC) as an easy method for identifying cell-SELEX targets.[45] However, SILAC confers significant additional cost to cell culture, and requires an initial pilot mass spectrometry analysis to optimize conditions prior to SILAC experiments.[45,64]

In the context of identifying aptamer targets, the term affinity purification has a dual meaning: the aptamer itself is an affinity ligand, but in order to capture target-bound complexes the aptamer must harbor an affinity tag with a well-defined binding partner. Biotin and the avidin-based proteins are commonly used for this task[65] as biotin's small size makes it ideal for nucleotide modification. The streptavidin-biotin interaction has a K_d in the femtomolar range and is resistant to changes in temperature, pH, and high

concentrations of salts and detergents frequently utilized in cell lysis and protein purification.[32,66] Streptavidin-conjugated resins, such as agarose or magnetic beads, enable capture of the biotinylated ligand and the proteins that associate with it.

Affinity purification experiments follow a generally recognized set of methods. Typically, cells or cell lysates are incubated with an affinity-tagged/labeled "bait" molecule (in this case a biotin-labeled aptamer). The bait molecules then associate with their "prey" proteins, which are "pulled-down" via capture of the affinity tag by incubation with purification resin. Purification resins most commonly consist of either agarose or magnetic particles that are surface-functionalized with moieties that specifically bind their cognate affinity tags. A portion of cell lysate used for each pull-down assay is reserved (referred to as the input fraction) prior to addition of purification resin, which allows for characterization of the starting material and direct comparison to purified fractions eluted later (referred to as pull-downs or eluates). After incubation with purification resin, a portion of the resulting lysate may be retained as the fraction that did not bind to the resin (referred to as the unbound fraction). Running these 3 samples side by side on SDS-PAGE gels for staining and blotting provides valuable insight into success or failure of experiments. If protein loading was significantly different, densitometry may be performed to determine enrichment between different sample types or treatments. The utility of the unbound fraction is twofold: it can reveal depletion of proteins compared to the input, and it can also reveal if sufficient purification resin was used, or how successful one particular elution scheme was to another.

2. MATERIALS AND METHODS

2.1. Reagents

Tris base, glycine, sodium hydroxide, methanol, sodium bicarbonate, sodium chloride, potassium chloride, ammonium sulfate, DMSO, acetic acid, isopropanol, boric acid, β-mercaptoethanol, and formaldehyde were purchased from Fisher (Waltham, MA). Triton X-100, Coomassie brilliant blue G-250, phosphoric acid, HEPES, PMSF, and MTT reagent were purchased from VWR (Radnor, PA). Magnesium chloride, IGEPAL-CA-630, 10× DPBS, BSA, DTT, EDTA, ammonium persulfate, sodium carbonate, L-glutamine, glycerol, penicillin/streptomycin solution, and glucose were purchased from Sigma (St. Louis, MO). Acrylamide solution (30%, 37.5:1 acrylamide:bis-acrylamide ratio), sodium dodecyl sulfate (SDS), 2× Laemmli sample buffer, PVDF, nitrocellulose, and TEMED were purchased from Bio-Rad (Hercules, CA). Streptavidin Dynabeads, HALT protease inhibitor cocktail, cell surface protein isolation kit, NeutrAvidin-HRP, SuperSignal West Pico, and EZ-Link NHS-LC-Biotin were purchased from Thermo (Waltham, MA). MDA-MB-231 cells, GelRed (Biotium, Fremont, CA), O′RangeRuler (Thermo), and Prism Ultra Protein Ladder (Abcam, Cambridge, UK) were kind gifts from Dr. T. Betancourt. Rabbit anti-Actin (A2066, Sigma) and goat-anti-rabbit-HRP antibodies were kind gifts from Dr. D. Garcia.

2.2. Aptamers

All oligonucleotides were purchased from Integrated DNA Technologies (IDT), resuspended to 100 μM in nuclease free water, divided into 10 μL aliquots among 0.5 mL tubes and frozen at -80 °C. In addition to TLS11a, a non-targeting aptamer, TD05, was used as a control probe for some experiments. The TD05 aptamer listed here was used as a mimic for the presence of DNA with both double-stranded and single-stranded regions- a characteristic of TLS11a. Fluorescence microscopy was used to confirm that TD05 did not bind to any of the cell lines used in the studies described here (data not shown). The sequences of these oligonucleotides are given in Table 2.

Table 2. Aptamer sequences.

Aptamer	Sequence
TLS11a	5′-ACA GCA TCC CCA TGT GAA CAA TCG CAT TGT GAT TGT TAC GGT TTC CGC CTC ATG GAC GTG CTG-3′
TD05	5′-CAC CGG GAG GAT AGT TCG GTG GCT GTT CAG GGT CTC CTC CCG GTG-3′

The aptamers used in these studies were synthesized with functional modifications to enable attachment to NPs, fluorescence imaging, and affinity purification. The nomenclature used throughout this work refers to aptamers with specific modifications used in each instance: Table 3 comprises a list of these abbreviated names and associated modifications. Chemical structures of each modification, and the context of attachment location within oligonucleotides is shown in Figure 6.

Table 3. Aptamer abbreviations and corresponding modifications. Sites of attachment are noted for each modification. Fluorescein is linked to an internal deoxythymidine (dT).

Aptamer Abbreviation	Functional Group	Fluorophore
TLS11a-Fluor	5′-NH_2	dT Fluorescein
Biotin-TLS11a	5′-Biotin	None
desBio-TLS11a-Fluor	5′-Desthiobiotin	dT Fluorescein
TD05-Fluor	5′-NH_2	dT Fluorescein

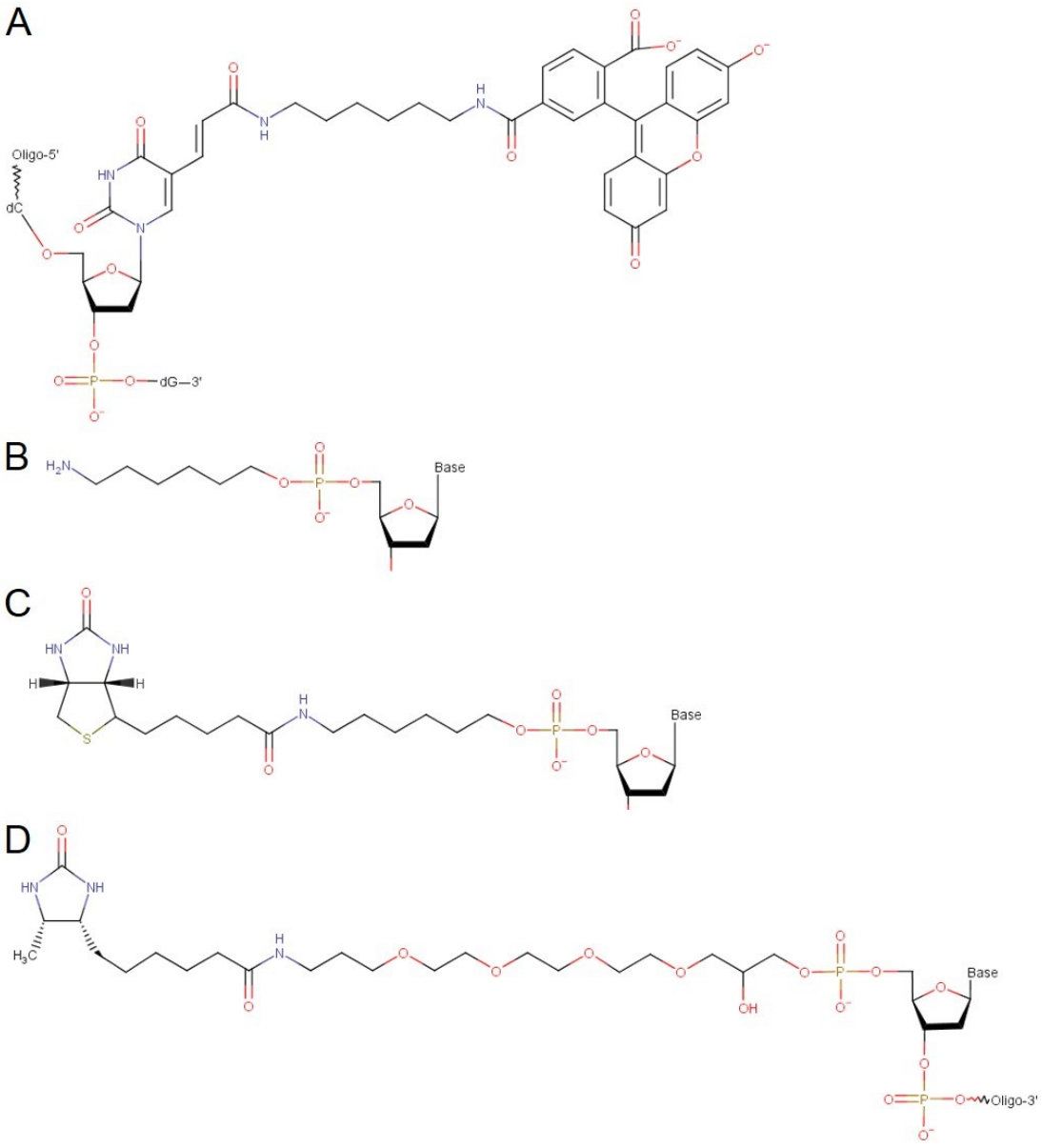

Figure 6. Structures of aptamer modifications. (A) Fluorescein-modified dT nucleotide shown in sequence context of TLS11a-Fluor. The location of the dT-Fluorescein in TD05-Fluor is the same as in TLS11a except that TD05 has a dG in place of the indicated dC. The dT-Fluor is penultimate to the 3′ terminal dG nucleotide of both aptamers. (B) Primary amine functional group and (C) biotin affinity tag, respectively, attached via C6 linkers to 5′ terminal phosphate. (D) Desthiobiotin affinity tag attached via TEG linker to 5′ terminal phosphate. Structures were drawn with MarvinSketch.

2.3. Thermal Melting Analysis

Experimental determination of TLS11a melting temperature (Tm) was performed

with a Jasco V-730 UV-Vis spectrophotometer equipped with a peltier controller. Biotin-TLS11a was diluted from stock to 1 μM, 2 μM, and 5 μM in DPBS containing 5 mM $MgCl_2$. Samples were prepared in triplicate, and aliquots of 110 μL were added to individual wells of an 8-well 1-cm path length quartz cuvette (Jasco) and closed with PTFE stoppers. Absorbance measurements at 260 nm were collected across a temperature range of 15 °C to 80 °C at a ramp rate of 1 °C per minute for both melting and annealing. Determination of Tm was performed with SigmaPlot. Scatter plots of raw melting data were analyzed with non-linear regression to generate curve fits. Second derivatives were calculated from each curve, and the inflection points of each were averaged to attain a Tm.

2.4. Tissue Culture

Mouse HCC cells, BNL 1ME A.7R.1 (MEAR) and normal mouse hepatocytes, BNL CL.2 (CL.2) were purchased from ATCC (Manassas, VA). MEAR and CL.2 cells were grown in DMEM:F12 (Corning, 90-090-PB) prepared to 1x concentration from powder in mQ water, containing the following: 10% FBS (Corning, 35-011-CV); 2.438 g/L $NaHCO_3$ (Fisher, BP328-1); 2.5 mM L-glutamine (Sigma, G7513); 100U penicillin, 0.1 mg/mL streptomycin (used from 100x solution, Sigma, P0781-20ML); 5 μg/mL insulin, 5 μg/mL transferrin, 5 ng/mL selenium (used as 1000x from solution, Lonza, 17-838Z); 40 ng/mL dexamethasone (Sigma, D4902-25MG); 50 ng/mL EGF (Sigma, E4127-5X.1MG). MDA-MB-231 cells were grown in DMEM:F12 containing the same concentrations of FBS, $NaHCO_3$, L-glutamine, and penicillin/streptomycin solution. All medium components were stirred together in tissue culture dedicated glassware and

filtered with sterile single-use 0.2 μm PES membrane filter top flasks. Cells were grown in T-25 and T-75 filter-top culture flasks at 37 °C in a %5 CO_2 humidified incubator. Cells were dissociated for passaging by washing with one media-volume of Versene (0.5 mM EDTA, sterile filtered), and incubated for 3 min at RT. Versene was aspirated, and 1/3 media volume of TrypLE (Thermo) was added to flasks and incubated at 37 °C for ~5 min, until ~90% of cells became detached as judged visually under the microscope. Dissociated cells were recovered in ½ media-volume of complete medium and then counted. Aliquots of suspended cells were removed, and 50 μL of cell suspension added to 50 μL Trypan blue (Sigma), and 10 μL of this solution was used for counting on a hemocytometer. For plating of cells into 96-well plates prior to MTT assays, or preparation of cells for freezing, cell suspensions were passed through 40 μm cell strainers (VWR) prior to counting to remove clumps of non-dissociated cells. Freezing media for all cell lines consisted of complete growth medium with 5% DMSO.

2.5. MTT Cytotoxicity Assays of HCC-Targeted Nanoparticles

The cytotoxic efficacy of TLS11a-functionalized NPs was tested in MEAR and CL.2 cells. Synthesis and characterization of NPs was done by collaborators (C. Munoz, Betancourt Lab) and has been reported.[53,67,68] A cartoon schematic of NPs used in these studies (Figure 7) illustrates aptamer functionalization and drug release.

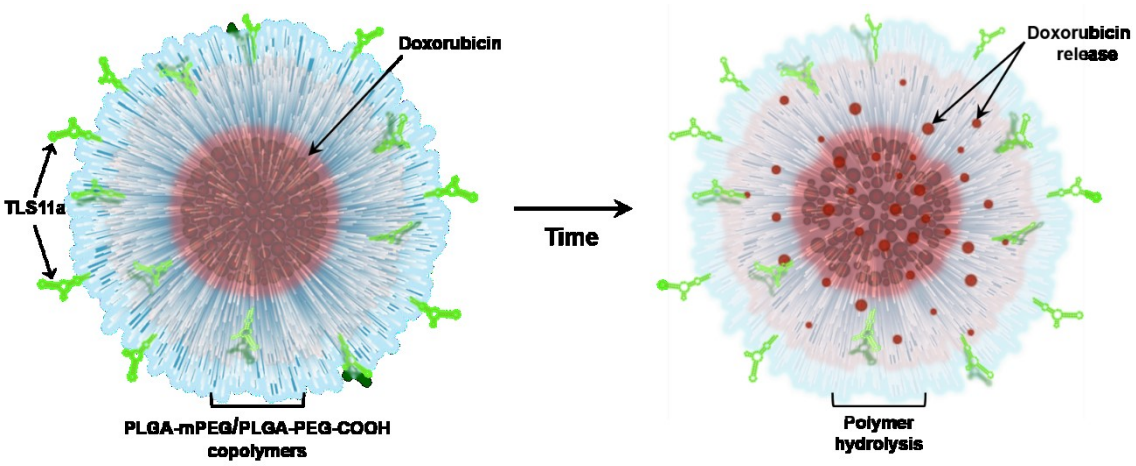

Figure 7. Depiction of drug release from TLS11a aptamer-functionalized biodegradable NPs. The NPs shown contain a hydrophobic core, which is loaded with the chemotherapeutic drug doxorubicin. Drug is released from the NPs over a period of ~36 hours. Active targeting to HCC is guided by TLS11a attached to the surface of the NPs. The biodegradable polymer eventually undergoes hydrolysis and can be eliminated by physiological processes.

General cell culture conditions are described in section 2.4. For these studies, cells were seeded into 96-well plates at approximately 1×10^4 cells/cm^2 (3,000 cells per well). Volumes of culture media, experimental treatments, and reagents added to cells were all 100 µL per well. Eight-channel pipettors were used for all liquid manipulations, and the sequence of pipetting across each 96-well plate was maintained for the duration of each study. For each experiment, one 96-well plate was used for each cell line and treatment condition, with one column in each plate dedicated to negative cytotoxicity control (media change in place of treatment) and positive cytotoxicity control (incubation with methanol for 15 minutes prior to final assay), respectively. After plating, cells were incubated for 48 hours to allow for attachment. Culture media was then removed and the following treatments were applied: TLS11a-functionalized NPs loaded with doxorubicin (Dox), blank NPs (no aptamer) loaded with doxorubicin, TLS11a-functionalized NPs (no Dox), blank NPs (no aptamer, no Dox), and doxorubicin alone. Each treatment was

diluted into complete culture medium and added to cells at a gradient of concentrations with respect to doxorubicin. For the NP groups without doxorubicin, treatments were diluted according to equivalent concentrations of NPs (in mg/mL). Plates were incubated with treatments for 4 hours, after which treatment media was carefully removed, replaced with complete culture medium, and plates incubated for an additional 48 hours. Cell viability following this procedure was determined by assessing redox potential with methylthiazolyldiphenyl-tetrazolium bromide (MTT) assays. Fresh assay reagent was prepared by dissolving MTT powder in DPBS to a final concentration of 0.5 mg/mL. Culture medium was carefully removed, MTT reagent added, and plates incubated at 37 °C and 5% CO_2 for 2 hours. The resulting solution was removed with particular caution to avoid disturbing any cells or formazan crystals. Alkalized DMSO (16 mM NH_4OH in DMSO) was added to plates, which were securely placed on an orbital shaker until all formazan crystals were solubilized. Absorbance was read on a BioTek plate reader (Winooski, VT) at 555 nm and 700 nm, for formazan and background, respectively. For each plate, background-subtracted absorbance values were normalized to the negative cytotoxicity (media change) control. Each set of experiments was carried out on the same day with the same batches of NP preparations/dilutions.

In addition to assays with NPs, control experiments were done in which cells were treated with dilutions of TLS11a-Fluor alone, NPs alone, and doxorubicin alone. This established working ranges and cellular responses for each component of the functionalized, drug-loaded NPs.

2.6. Aptamer-Target Pull-Down Assays

Aptamer-target pull-down assays were performed under a variety of conditions to optimize for cell lysis and target capture. Methods and buffers tested were selected from previous studies that identified cell-SELEX aptamer targets.[39,45,58,61] The optimized procedures are described in sections 2.6.1-2.6.4, and the buffers used and their compositions are listed in Table 4.

Table 4. List of buffers used in pull-down assays.

Buffer	Component	Final Concentration	pH
Labeling Media	Complete culture medium desBio-TLS11a-Fluor*	1× 100 nM	n/a
DVS Wash Buffer	DPBS with Ca^{2+} and Mg^{2+} $MgCl_2$ Glucose	1× 5 mM 4.5 g/L	Physiological†
$DPBS^{+}Mg$	DPBS with Ca^{2+} and Mg^{2+} $MgCl_2$	1× 5 mM	Physiological†
Crosslinking Solution	$DPBS^{+}Mg$ Formaldehyde*	1× 1% (v/v)	Physiological†
LB-C Lysis Buffer	HEPES NaCl KCl $MgCl_2$ Triton X-100 Sodium deoxycholate Glycerol EDTA DTT* PMSF* HALT Protease inhibitors*	50 mM 150 mM 5 mM 5 mM 2% (v/v) 0.1% (w/v) 5% (v/v) 1 mM 0.5 mM 1 mM 1×	7.9
2× Sample Buffer	Tris-HCl Glycerol SDS Bromophenol blue β -mercaptoethanol*	62.5 mM 25% (v/v) 2% (w/v) 0.01% (w/v) 5% (v/v)	6.8
1× Sample Buffer††	Tris-HCl Glycerol SDS Bromophenol blue β-mercaptoethanol*	31.25 mM 12.5% (v/v) 1% (w/v) 0.005% (w/v) 2.5% (v/v)	6.8

* Added at immediate time of use
† Exact value not specified by manufacturer, listed range pH 7.0 – 7.4
†† Diluted from 2× with mQ H_2O

2.6.1 *In situ* Labeling of Live Cells with TLS11a

Two T-75 flasks of each cell line were grown to ~80% confluence under described culture conditions. Labeling media was made immediately prior to use: stocks of 100 μM desBio-TLS11a-Fluor were diluted to 100 nM in 10 mL cold (4 °C) complete culture medium in sterile 15 mL conical tubes and inverted to mix well. Culture medium

was aspirated from each flask, and 5 mL of cold labeling media was added to each flask. Importantly, after the initial addition of cold medium, flasks were kept cold at all times, and all buffers and reagents exposed to cells were ice cold. Cells were incubated with labeling media at 4 °C for 1 hour with occasional rocking. After incubation, labeling media was aspirated, and cell monolayers were washed twice with 10 mL of DVS wash buffer, and once with $DPBS^{+}Mg$. One of each pair of flasks was visibly marked to indicate that it would be used for crosslinking, and 10 mL of $DPBS^{+}Mg$ containing 1% formaldehyde was added to the marked flask. The unmarked flask received 10 mL of $DPBS^{+}Mg$, and both flasks were incubated at 4 °C for exactly 10 minutes. Formaldehyde and $DPBS^{+}Mg$ solutions were promptly aspirated, after which each flask was immediately washed 3 times with 10 mL of $DPBS^{+}Mg$.

As a control for the manipulation of cells during the labeling protocol, an identical procedure was performed in which the only difference was that cold media added to cells did not contain TLS11a.

2.6.2 Fluorescence Microscopy

After the labeling procedure, flasks with cell monolayers were nested flat on ice, and underwent brief (<3 min) excursions to RT to be imaged for fluorescence and transmitted light on an EVOS® FL Auto Imaging System inverted microscope (Life Technologies). Images were taken with a 10× (NA 0.40, Olympus) objective lens. Both transmitted light and fluorescence images were acquired for each field of view. A GFP light cube (470/22 nm excitation, 510/42 nm emission) was for green channel imaging. Gain, light intensity, and exposure times were kept consistent for all images acquired.

ImageJ was used for image adjustment of brightness/contrast, and identical adjustments were applied to all images.

2.6.3 Harvesting Cells

The final volume of $DPBS^{+}Mg$ was aspirated from each flask of cells and 1 mL of LB-C lysis buffer was added to each. Flasks were kept on ice and rocked to keep cells bathed in lysis buffer until edges of monolayers began to curl. Cells were finally harvested by scraping, transferred to low-retention 1.5 mL tubes on ice, and pipetted to break up clumps. One mL Wheaton glass dounce homogenizers with tight pestles (0.025 - 0.076 mm clearance) were triple rinsed with mQ H_2O, placed in ice, and rinsed with 1 mL of LB-C. Excess LB-C was aspirated from homogenizers, cell suspensions added to each, and homogenized for 7 – 15 minutes (depending on cell line and treatment type) until >90% of cells were disrupted. Lysis was judged by removing 5 µL aliquots periodically during homogenization and placed on microscope slides observed at 25× magnification. Lysates were carefully pipetted into chilled 1.5 mL tubes and centrifuged at 750 ×g for 5 min at 4 °C. Supernatants were transferred to fresh 1.5 mL tubes and centrifuged again for 10 min at 10,000 ×g at 4 °C. The final resulting supernatants were moved to fresh 1.5 mL tubes.

2.6.4 Pull-Downs

Fifty µL was removed from each clarified lysate and reserved as the input fraction. An equal volume of 2× SB was added to each input, vortexed briefly, and incubated at 95 °C for 5 min in a heating block. Tubes were placed on ice to allow vapor

to condense, quick-spun in a microcentrifuge (10 sec), vortexed briefly, then frozen at -80 °C. A sufficient volume of MyOne Streptavidin T1 Dynabeads (Thermo) for the number of pull-downs immediately being performed was added to a 1.5 mL tube. Beads were captured on a DynaMag-2 magnet (Thermo) for 1 min, and storage buffer aspirated. Subsequently, beads were washed 3 times: 1 mL LB-C was added to the beads, tubes rotated end-over-end at 4 °C for 5 min, beads captured for 1 min, and wash aspirated. Beads were resuspended in the initial bead volume (BV) of LB-C, and 25 µL was added to each clarified lysate. Tubes were sealed with parafilm and rotated end-over-end at 4 °C overnight. The following day, tubes were briefly spun in a picofuge to release beads and lysate from caps. Beads were captured for ≥1 min, until lysates appeared entirely clear, supernatants were removed to fresh 1.5 mL tubes and reserved as unbound fractions. Target-bound beads from each pull-down were washed 3 times: 1 mL LB-C was added, tubes briefly vortexed (~5 sec), rotated end-over-end at 4 °C for 5 min, beads captured for ≥1 min (as above), and aspirated. After the final wash, tubes were spun briefly in a picofuge to collect any residual liquid on the sides of the tubes, beads captured, and aspirated. Two BVs (50 µL) of 1x SB prepared with sterile mQ H_2O was added to each pull-down and vortexed briefly. Fifty µL aliquots from each unbound fraction were transferred to an equal volume of 2x SB in fresh tubes. All samples were immediately incubated at 95 °C for 5 min in a heating block. Tubes were placed on ice to allow vapor to condense, quick-spun in a microcentrifuge (10 sec), and vortexed briefly. Beads in pull-downs were captured for 2 min and eluates were transferred to chilled low-retention 1.5 mL tubes. Any samples that were not used immediately were frozen at -80 °C.

2.7. SDS-PAGE

Pre-cast 8-16% TGX Stain-Free SDS-PAGE gels (Bio-Rad) were used in initial experiments, and are indicated where used. Otherwise, gels were poured by hand in glass plates with a Bio-Rad gel casting system. Gel and buffer compositions are listed in Table 5.

Table 5. List of buffers used in SDS-PAGE.

Component	Reagent	Final Composition
TGS Running Buffer	Tris-base Glycine SDS	25 mM 192 mM 10% (w/v)
Separating Gel	1.5 M Tris-HCl, pH 8.8 30% Acrylamide (37.5:1) 10% SDS 10% APS TEMED	25% (v/v) Variable 1% (v/v) 1% (v/v) 0.1% (v/v)
Stacking Gel	1 M Tris-HCl pH, 6.8 30% Acrylamide (37.5:1) 10% SDS 10% APS TEMED	12.6% (v/v) 16% (v/v) 1% (v/v) 1% (v/v) 0.1% (v/v)

Protein samples were diluted 1:1 with 2× sample buffer (see Table 4), incubated in a heating block at 95 °C for 5 minutes, cooled, and briefly centrifuged to collect condensation. Broad range (Bio-Rad) protein molecular weight (MW) standard was used until the lot was consumed. Subsequently, Prism Ultra Protein Ladder (Abcam) was used. Annotations in results reflect manufacturers' corrected observed molecular weights for Tris-glycine running buffer.

2.8. Western and Aptamer Blotting

Transfer of PAGE gels to PVDF-LF (Bio-Rad) or 0.45 µm nitrocellulose (Bio-Rad) membranes was optimized according to acrylamide percentage. Prior to transfer, gels were rinsed briefly with mQ water to remove residual SDS, then wetted in ice cold transfer buffer (see Table 6 for buffers). Transfer sandwich stacks were prepared in ice-cold transfer buffer; sponges and filter papers were saturated prior to assembly, and nitrocellulose membranes were equilibrated by submerging in cold transfer buffer, while PVDF membranes were first activated in pure methanol before equilibration. For all transfers, a frozen ice-pack (-20 °C) was added to the tank, which was moved to 4 °C for the duration of electroblotting. Transfer of 10% gels was carried out at constant 250 mA for 2.5 hours; 12% gels at 300 mA for 1 hour.

Table 6. List of buffers used in western and aptamer blotting.

Buffer	Component	Final Composition	Use
Transfer Buffer	Tris-base Glycine Methanol	25 mM 192 mM 10% (v/v)	Electroblotting
Ponceau Stain	Ponceau S Glacial acetic acid	0.1% (w/v) 5% (v/v)	Staining protein in membranes
TBST	Tris-base NaCl KCl Tween-20	25 mM 150 mM 2 mM 0.1% (v/v)	Diluent and wash for western blots
5% NFDM	NFDM TBST	5% (w/v) 1x	Western blocking
0.5% NFDM	5% NFDM TBST	1% (v/v) 1x	Western 1° and 2° diluent
3% BSA/ DPBS^{+}Mg	BSA DPBS with Ca^{2+} and Mg^{2+} $MgCl_2$	3% (w/v) 1× 5 mM	Aptamer blocking
0.3% BSA/ DPBS^{+}Mg	3% BSA/ DPBS^{+}Mg DPBS with Ca^{2+} and Mg^{2+}	10% (v/v) 90% (v/v)	Aptamer and 2° diluent
0.1% BSA/ DPBS^{+}Mg	BSA DPBS with Ca^{2+} and Mg^{2+}	0.1% (w/v) 1×	Wash for aptamer blots

Upon completion of electroblotting, sandwiches were disassembled and membranes placed in small, clean, plastic boxes where they were rinsed very briefly in mQ H_2O to remove residual transfer buffer. Ponceau solution was added to each box, and membranes incubated with shaking for 5 min at RT. Staining solution was discarded, and membranes were destained with successive rinses of mQ H_2O until lanes with protein appeared bright pink against a white background. Wet membranes were trimmed with cleaned surgical scissors to reflect only the area of the membrane occupied by the gel, then positioned in a plastic page protector and scanned. Subsequently, membranes were returned to boxes and completely destained with mQ H_2O before proceeding to blocking. Membranes were blocked for 1 hour at RT with shaking.

After blocking, membranes were placed into Kapak pouches (VWR), which were then cut to size for each membrane and closed with an impulse sealer on three sides. A sufficient volume of 1° antibody or aptamer solution was added to each bag to completely envelop the membrane, bubbles were removed, and bags were double-sealed on all sides. Pouches were incubated at 4 °C overnight on an end-over-end rotator or a 2-way rocking platform.

The following day, sealed pouches were carefully opened with clean surgical scissors, and membranes removed with flat-head forceps to clean plastic boxes containing respective wash buffer. Membranes were washed 3 times, shaking, at RT, 7 minutes per wash. After removal of the final wash, a sufficient volume (at least 15 mL) of 2° antibody solution was added to completely submerge the membranes in the boxes. Incubation was carried out with shaking at RT for 1 hour. Membranes were then washed 3 times as described above. After the final wash, membranes were placed on a clean page-protector and excess wash blotted away carefully with Kim-Wipes. For chemiluminescent imaging, a volume of ECL reagent (SuperSignal West Pico Chemiluminescent Substrate, Thermo) sufficient to entirely cover the membrane was prepared immediately before use, pipetted directly onto the membrane, and incubated at RT for 5 minutes. ECL reagent was removed and excess blotted with Kim-Wipes. Page protectors were closed over the membranes to keep them wet, and bubbles removed prior to placement on imaging instrument. Chemiluminescence signals were acquired with a ChemiDoc imager (Bio-Rad) or a GeneGnome imager (Genesys). Epi-illuminated images of each membrane were acquired after chemiluminescence detection for determination of membrane alignment for subsequent image processing. Membranes being scanned for fluorescence

were air dried, then scanned on a PharosFX Plus imaging system (Bio-Rad). Images from the ChemiDoc were exported as raw data from native format to TIFF files; images from the GeneGnome were saved as TIFF files.

2.9. Colloidal Blue Gel Staining

Colloidal Coomassie brilliant blue G-260 (CBB G-250) staining solution (Table 7) was prepared by adding 2.5 mL of stock solution B to 100 mL of stock solution A in a clean glass bottle and stirring as strongly as possible on a magnetic stir plate for 20-30 minutes. To this solution, 25 mL of pure methanol was added, and strong stirring continued for an additional 30 minutes. Prior to staining, 1 mm gels placed in clean plastic boxes and rinsed in mQ water for ~30 minutes (3× 10 min) to remove SDS, which affects sensitivity of colloidal blue staining [69]. 1.5 mm gels were incubated in methanol (destain solution) for 10 minutes, then washed in mQ water as above. After washes, freshly prepared colloidal staining solution was poured over gels to completely submerge (75 – 100 mL), boxes were covered with lids, and incubated overnight at RT on an orbital shaker. Staining solution was discarded, and precipitated particles wiped from plastic boxes with Kim-Wipes soaked in destain solution. Gels were then covered in destain to submerge, and incubated with shaking until background was satisfactorily reduced. Gels were placed in page-protectors for scanning, then returned to boxes containing mQ water. After equilibration in water (at least overnight), selected gels were dried between cellulose sheets on a gel drying platform (Bio-Rad).

Table 7. List of solutions used in colloidal blue gel staining.

Solution	Reagent	Composition
Stock Solution A	Ammonium sulfate Phosphoric acid	10% (w/v) 2% (v/v)
Stock Solution B	CBB G-250 mQ water	5% (w/v) Solvent
Staining Solution	Solution A Solution B Methanol	100 mL 2.5 mL 25 mL
Destain Solution	Methanol mQ water	25% 75%

2.10. Fluorescent Imaging of Gels and Membranes

Membranes and SDS-PAGE gels were scanned on a PharosFX Plus system (Bio-Rad) equipped with a 488 nm laser line and a 530 nm bandpass filter. Images were acquired at 50 µm resolution with laser intensity sufficient to obtain unsaturated signal. Membranes were allowed to dry prior to imaging. SDS-PAGE gels were rinsed briefly with mQ water to remove residual SDS after removal from gel plates and scanned immediately. Raw data images were exported from native format to TIFF files.

2.11. Stained Gel and Membrane Scanning

All colloidal blue stained gels and Ponceau stained membranes were scanned in dedicated sheet protectors. Images were acquired at 300 or 600 dpi in 48-bit color and saved as TIFF files.

3. RESULTS AND DISCUSSION

3.1. Structure Prediction and Thermal Melting Analysis of TLS11a

The predicted Gibbs free energy (ΔGs) of folding for TLS11a were evaluated under various parameters with respect to salt concentrations and temperatures. Results were consistent between Integrated DNA Technology's UNAFold tool and the mfold web server.[70] In the presence of 150 mM NaCl and 5 mM $MgCl_2$ at 4 °C, the conditions at which cell-SELEX was performed by Shangguan *et al*., the ΔG of folding is predicted to be -27.1 kcal·mol^{-1}.[46]

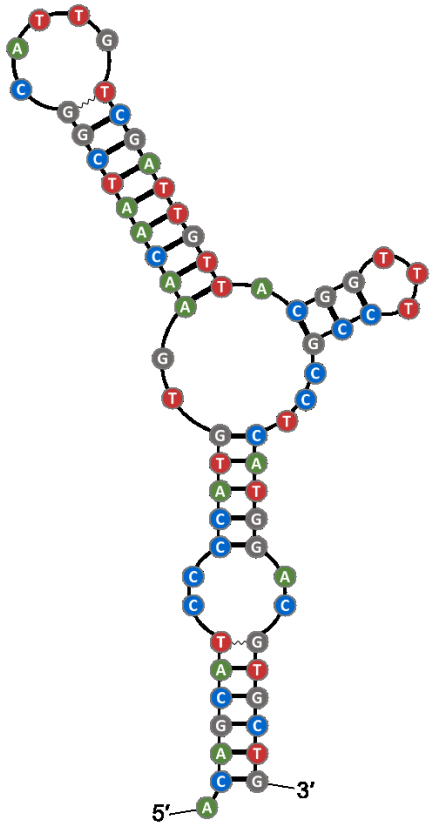

Figure 8. Predicted secondary structure of TLS11a. The sequence of TLS11a was entered into the IDT UNAfold tool and the mfold webserver to obtain a predicted secondary structure and associated calculated thermodynamic values of folding.

Importantly, when thermodynamic values were calculated at 37 °C, although the predicted ΔG increased to -10.25 kcal·mol^{-1}, the predicted secondary structure remained the same. This indicates that TLS11a likely maintains a stable conformation across the range of experimental conditions used throughout the studies reported here. The experimentally determined Tm of 57.04 °C (Figure 9) is in excellent agreement with the predicted Tm of 57.1 °C. These data provide evidence that Biotin-TLS11a folded into the structure predicted.

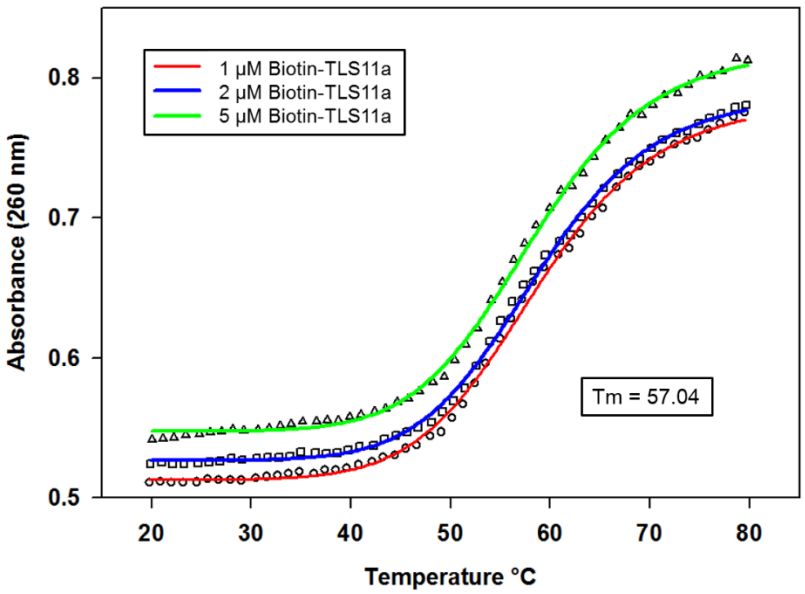

Figure 9. Thermal melting curves of Biotin-TLS11a.

3.2. MTT Cytotoxicity Assays

The dose-response tests established working ranges for targeted-NP efficacy studies. Free doxorubicin HCl (Figure 10) exhibited an effective working range of 50 µM to 0.78 µM after 4 hour incubation.

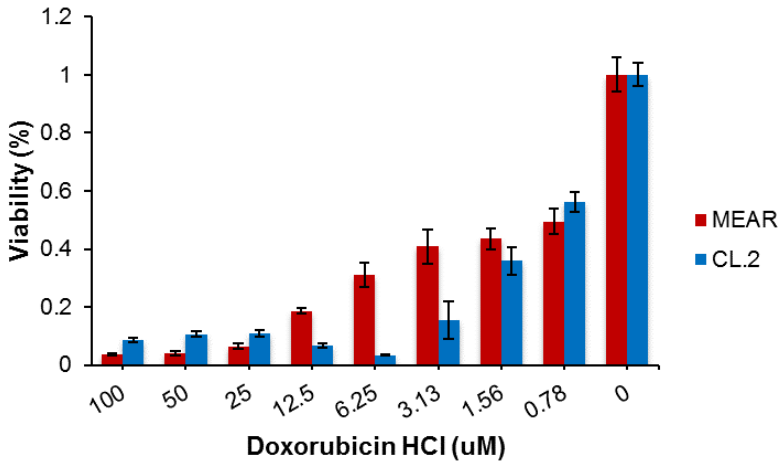

Figure 10. Dose response optimization of free doxorubicin in MEAR and CL.2 cells. Doxorubicin HCl was dissolved in DMSO and added to complete culture medium. Cells were treated for 4 hours, after which the media was removed and replaced with fresh culture medium and cells allowed to incubate for a further 48 hours. Error bars represent standard deviations.

Nanoparticles alone (no aptamer, no doxorubicin) began to display cytotoxicity on their own (Figure 11) at high concentrations. Given the reported Dox loading capacity of the NPs[53], the maximum concentration of Dox-loaded NPs used in drug delivery studies was well below the threshold at which NPs alone exhibited cytotoxicity.

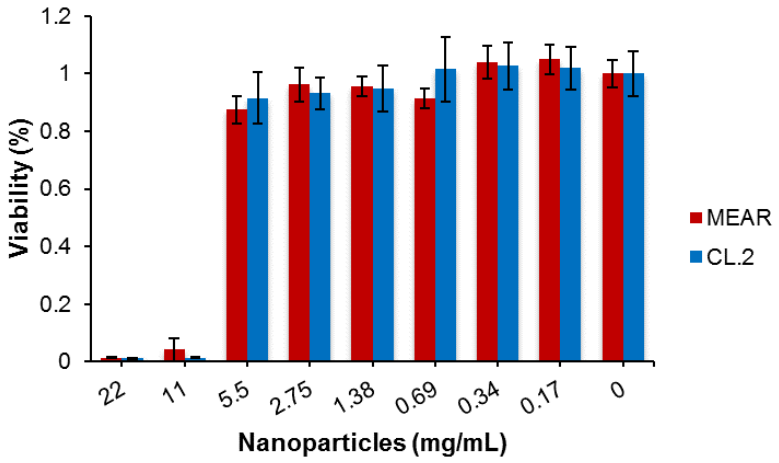

Figure 11. Blank nanoparticle cytotoxicity screen. Nanoparticles that did not contain doxorubicin or TLS11a were diluted in complete culture media, incubated, and tested as described for MTT assays. Error bars represent standard deviations.

Free TLS11a-Fluor (Figure 12) did not affect cell viability. The concentrations of aptamer used in this screen reflected the ranges which were present on functionalized NPs in drug-delivery studies.

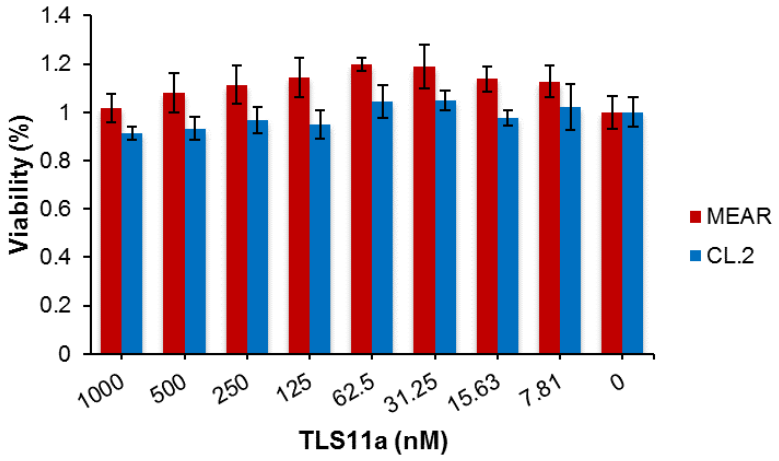

Figure 12. Effect of TLS11a-Fluor alone on cell viability. TLS11a-Fluor alone was diluted from stock into complete culture media, incubated, and tested as described for MTT assays. Error bars represent standard deviations.

In MEAR cells, TLS11a-functionalized NPs loaded with Dox performed as well as doxorubicin alone, while NPs containing Dox, but no aptamer, were not as effective (Figure 13). Neither NPs alone, or empty NPs functionalized with TLS11a, displayed significant cytotoxicity in these cells.

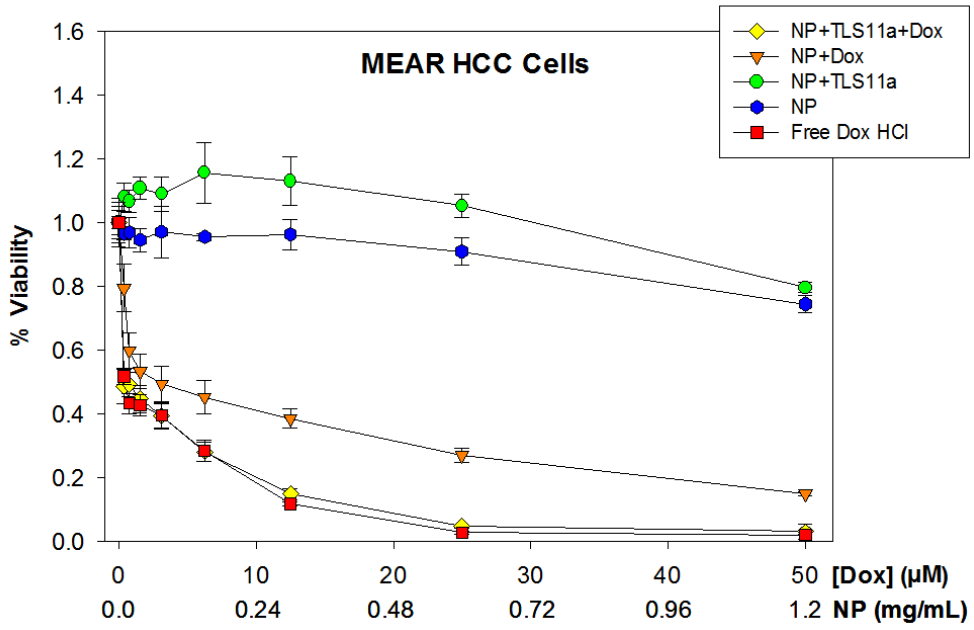

Figure 13. MTT cytotoxicity assay of NPs and free Dox HCl in MEAR cells. NP concentrations corresponding to each Dox concentration are given below the X axis.[53]

In normal hepatocytes, NPs with Dox but no TLS11a appeared to be most cytotoxic overall, followed by TLS11a functionalized NPs containing Dox, and free Dox. Although it was hoped that the TLS11a-targeted nanoparticles would exhibit specificity for HCC cells and produce lesser effects in normal cells, these data are still consistent with expected outcomes of treating cancer cells versus normal cells with a cytotoxic chemotherapeutic. Cancer cells can proceed through cell division in the presence of DNA damaging agents, while normal cells are programmed to undergo apoptosis in response to DNA damage. It is thus expected that the presence of doxorubicin, a DNA damaging

agent, in the culture environment of normal hepatocytes, would cause cell death regardless of the delivery vehicle employed.

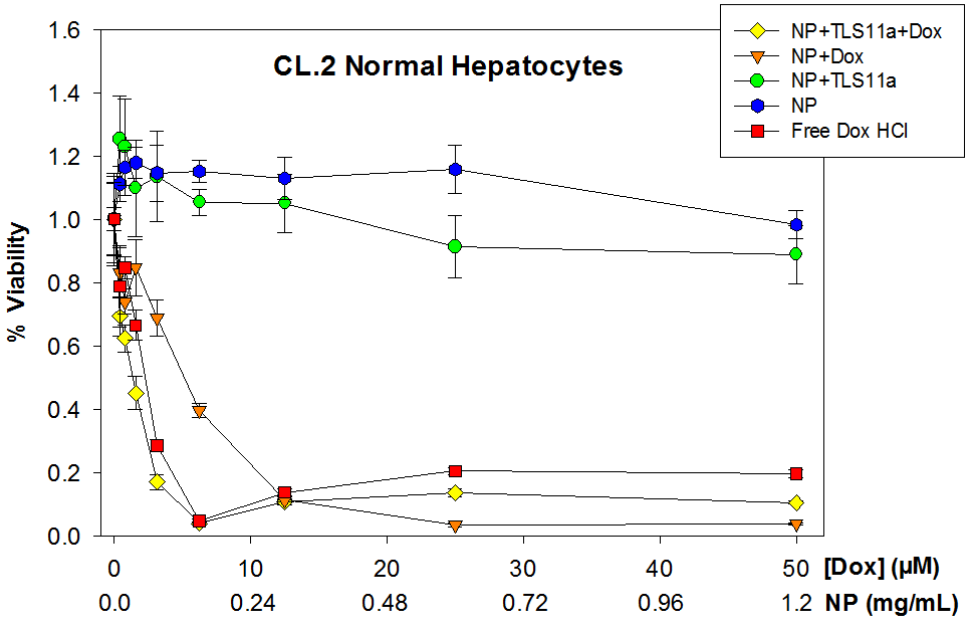

Figure 14. MTT cytotoxicity assay of NPs and free Dox HCl in CL.2 cells. NP concentrations corresponding to each Dox concentration are given below the X axis.

The efficacy of NP drug delivery systems relies largely on physiological phenomena that occur *in vivo*.[14] To fully assess the benefits of drug delivery via NPs, a functional circulatory system is a critical component to testing in disease models. These data were generated in a cell culture environment, and as such, without a system of vasculature or a source of flow in the cellular environment, even targeted NPs could be expected to exhibit cytotoxicity to normal cells. As drug is released from the NP, it permeates the media covering the cells, leading to an effect similar to what may be expected from treatment with free drug alone.

The trends in these data may also have been subject to a confounding effect from the inclusion of dexamethasone in cell culture medium. The composition of culture

medium we used was identical to that reported in the original TLS11a study by Shangguan *et al*.[46] The addition of dexamethasone inhibits spontaneous apoptosis in cultured primary hepatocytes, which may have been the rationale behind its use by their group.[71] However, the mechanism by which dexamethasone inhibits apoptosis is of importance here: dexamethasone stabilizes procaspase-3 expression correlating with reduced caspase-3 protease activity, and induces expression of Bcl-2, an anti-apoptotic effector.[71] The mechanism of doxorubicin's cytotoxic effect has been linked to decreased expression of Bcl-2 and induction of caspase-3 cleavage.[72,73] If dexamethasone countered the effect of doxorubicin in our studies, this suggests that experiments performed in the absence of dexamethasone may display different trends, however this needs to be determined experimentally.

3.3. Preliminary Data for TLS11a-Target Identification

Previous work indicated that TLS11a's cellular target was an approximately 21 kilodalton (kDa) protein.[48] This led to the hypothesis that the target was a cell surface protein due to its relatively low molecular weight, thus being unlikely to pass the cytosolic membrane (see Figure 5). In an effort to confirm this finding, whole cell extracts (WCEs) and preparations of cell surface proteins (CSPs), previously isolated from MEAR and CL.2 cells using a cellular fractionation kit (Thermo-Fisher), were run on 8-16% pre-cast TGX gels (Bio-Rad) and transferred to low-fluorescence polyvinylidene difluoride (LF-PVDF) membranes which were probed with TLS11a-Fluor and the non-targeting aptamer TD05-Fluor (Figure 15). The presence of a prominent ~21 kDa band in CL.2 protein fractions and both the TLS11a-Fluor and negative control

TD05-Fluor blots indicates that this signal was likely a result of non-specific binding. Additional non-specific signal is apparent in the TLS11a-Fluor blot of Figure 15, as a laddered banding pattern is present in both MEAR and CL.2 WCEs. However, a faint high MW band is visible above the 205 kDa marker in only the MEAR WCE. Given that this appeared to be the only specific band, the idea that the TLS11a target was potentially a membrane-spanning protein was revisited.

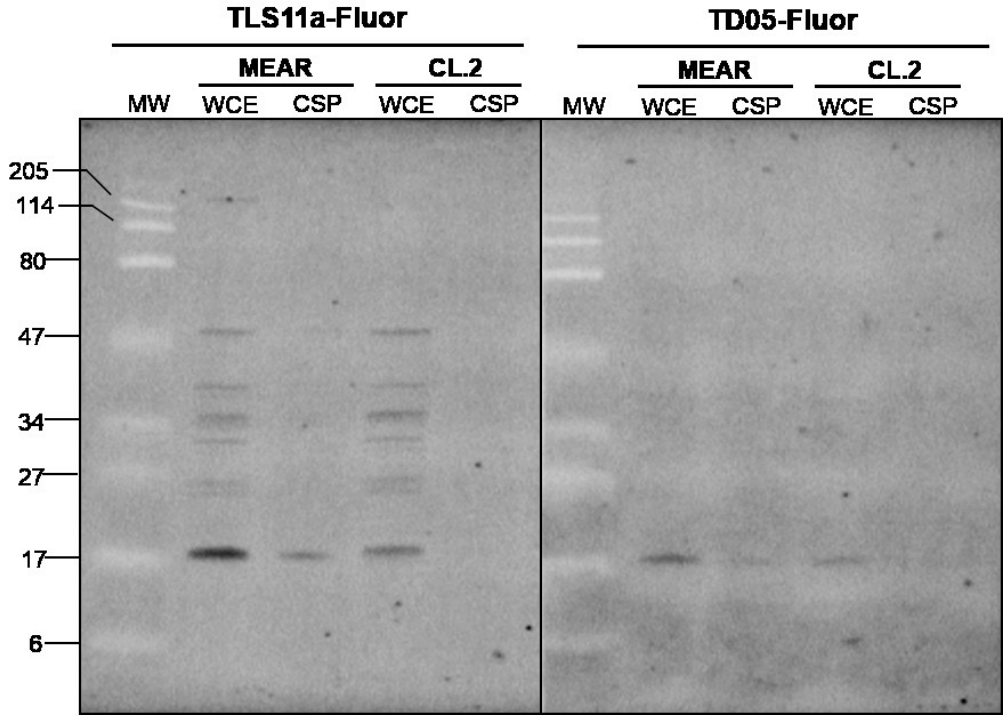

Figure 15. MEAR and CL.2 whole cell extracts and cell surface proteins blotted with fluorescent aptamers. Samples were run on an 8-16% gradient gel. Aptamers were diluted to 1 nM final concentration. MW, molecular weight; WCE, whole cell extract; CSP, cell surface proteins.

In an effort to achieve a preliminary identification of the specific TLS11a target using aptamer blotting, a pull-down assay using Biotin-TLS11a was developed. The rationale behind this approach was to (1) use a previously confirmed method of TLS11a labeling of whole cells,[48,53] and (2) enrich protein extracts for the TLS11a target as

reports by other groups have indicated that cell-SELEX evolved aptamers often recognize targets of relatively low abundance.[44,45,74]

The pilot pull-down assay was performed entirely *in vitro* by adding 100 nM Biotin-TLS11a to 1 mL of each MEAR and CL.2 cell lysates, as this version of the aptamer was in limited supply at the time. The same protein fractions in Figure 15 were run alongside input fractions (abbreviated "in") and pull-down eluates (abbreviated "PD") from this experiment, and blotted with fluorescent aptamers (Figure 16) to provide for direct comparison between new and previous results.

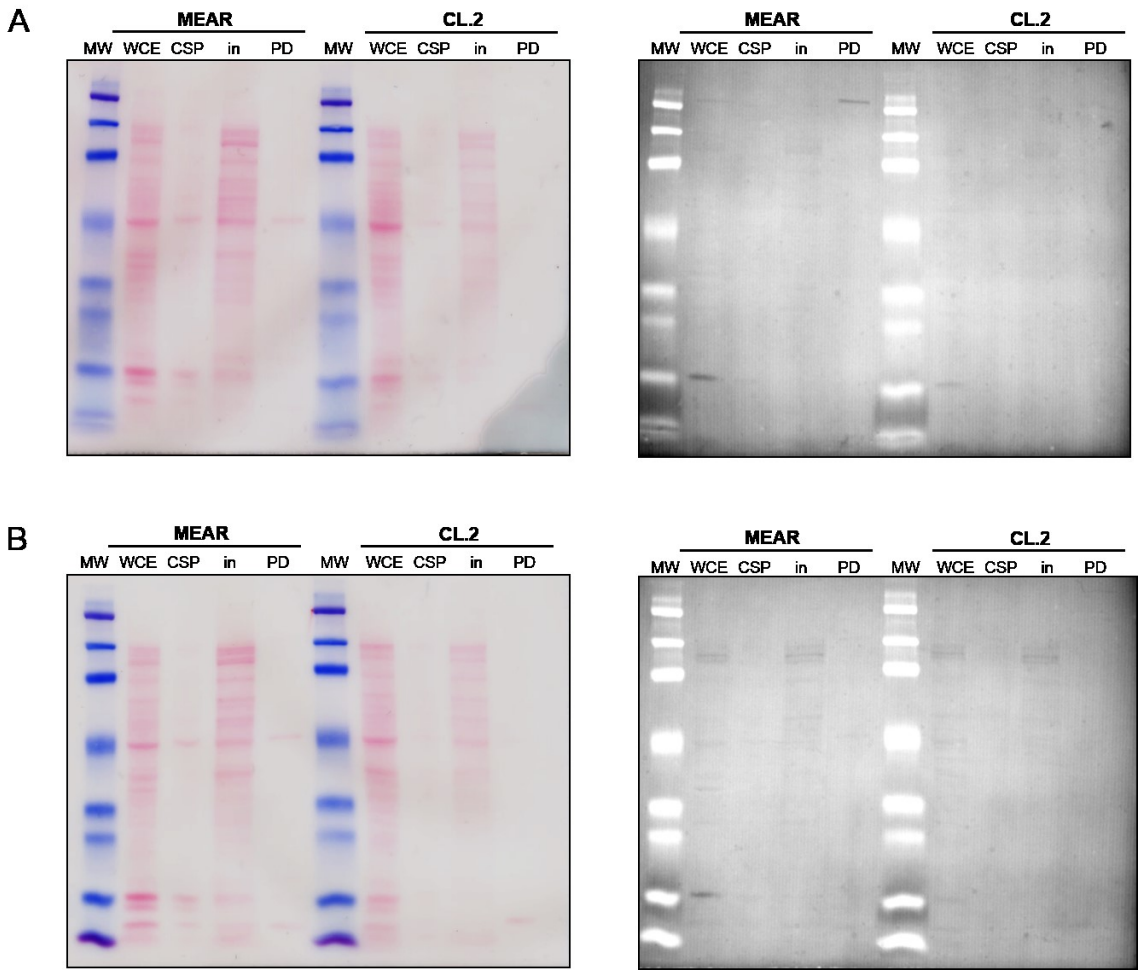

Figure 16. Fluorescent aptamer blots of MEAR and CL.2 cellular fractions and pull-downs. Samples were run on 8-16% gradient gels. (A) Left to right, Ponceau stain and corresponding TLS11a-Fluor blot. (B) Left to right, Ponceau stain and corresponding TD05-Fluor blot. Aptamers were diluted to 1 nM. Note the high MW band (just above the 205 kDa marker) in the right panel of (A), visible in the MEAR PD lane, and very faintly in the MEAR WCE lane. WCE, whole cell extract; CSP, cell surface proteins; in, input; PD, pull-down.

In spite of a unique band, high background and weak signal were a problem in these blots, obscuring quantification efforts. Even with the use of LF-PVDF membranes, this issue could not be resolved. The lack of reproducibility between these blots and previously reported data[48] showing good signal to noise ratio is not easily explained, although it is hypothesized that it was due in part to blotting with TLS11a-Fluor in these studies versus TLS11a with an AlexaFluor-546 tag in the previous work. Furthermore, attempts to blot for loading controls with antibodies followed by fluorescent secondary

antibody did not yield any meaningful results (data not shown), making direct comparisons and quantification impossible. It is primarily for this reason that Ponceau stains of all blots were scanned and are presented throughout this work. To ensure the methods being used were effective with antibodies, the protein preps in Figure 16 were run again and blotted with primary anti-actin (a commonly used protein loading control) and HRP-conjugated secondary for detection via chemiluminescence (Figure 17).

Actin was readily detected with chemiluminescence, verifying that the methods worked. The presence of a prominent band visible in Ponceau stains running just below the 47 kDa MW marker had been noted prior to blotting for actin. Ponceau stains were analyzed using migration of the MW standard as a reference, giving a calculated MW of 43 kDa for this band, the reported MW detectable with this actin antibody. In addition, it was noted that actin appeared in the CSP samples, and consistently appeared in pull-down eluates and their associated inputs.

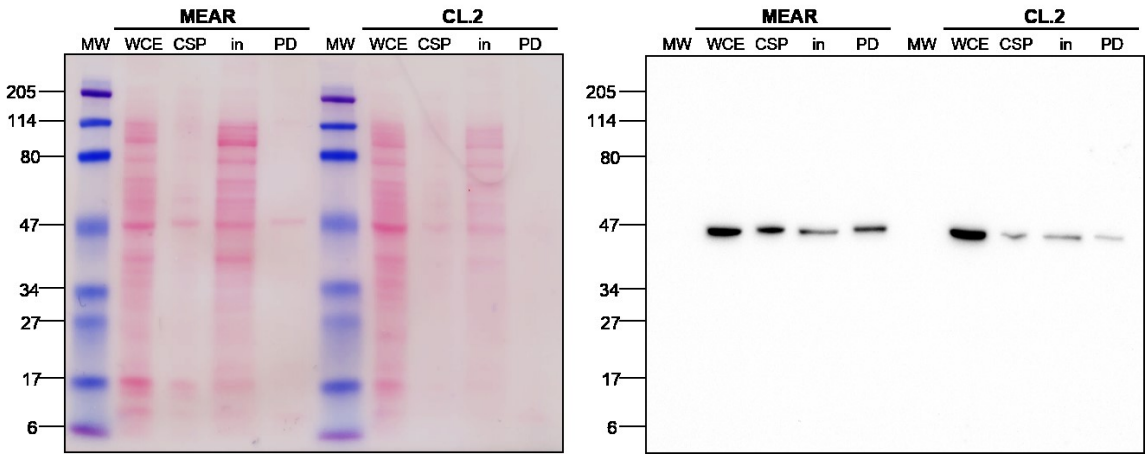

Figure 17. MEAR and CL.2 whole cell extracts, cell surface proteins, and pull-downs blotted for actin. Samples were run on an 8-16% pre-cast gradient gel. Primary actin antibody was diluted 1:1000; secondary HRP antibody was diluted 1:20,000. WCE, whole cell extract; CSP, cell surface protein; in, input; PD, pull-down.

With a detectable signal, unique to MEAR cell fractions in the fluorescent aptamer blots (Figure 16), and apparent success of the pilot pull-down assay, additional Biotin-TLS11a was obtained. Given the high MW of the observed unique band, lower percentage gels (10%, 37.5:1 linear to bisacrylamide ratio) were used in subsequent experiments to allow for better migration and separation of large proteins. Additionally, methods were adapted for chemiluminescent aptamer blotting with Biotin-TLS11a. The use of chemiluminescence in blotting techniques allows for potential improvements over fluorescence-based methods. Adjustment of exposure time (as opposed to adjustment of laser power/gain for fluorescence) allows for detection of low-abundance signals with good signal-to-background ratio without the drawback of fluorophore bleaching. The use of enzyme-conjugated secondary antibodies/recognition molecules inherently amplifies signal[75] (in correlation with sample abundance) which can further improve signal detection. Thus, aptamer blotting with Biotin-TLS11a was carried out using NeutrAvidin-HRP as the secondary detection molecule (Figure 18) followed by incubation with ECL substrate.

Keeping in mind that the target protein of interest may be a membrane protein, consideration was given to cell lysis conditions, as membrane proteins can be notoriously difficult to isolate. A set of lysis buffers containing detergents in varying ratios was tested in pull-downs from MEAR cells.

The signals in this blot differed from what was seen in previous fluorescent aptamer blots. Prominent bands at ~114 kDa and ~72 kDa were apparent, although no high MW band of ~205 kDa was detected as anticipated. Similarly to the fluorescent

blots, no signals were detectable in the inputs.

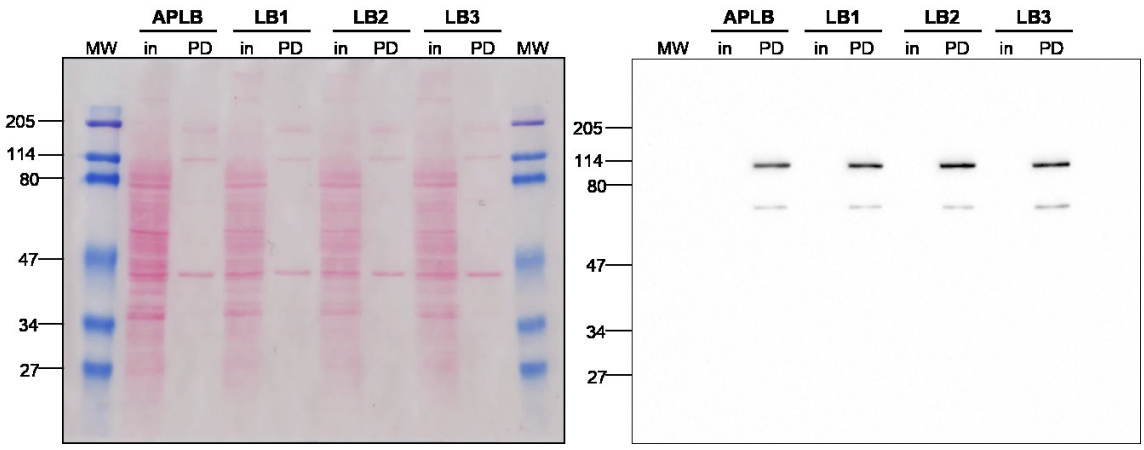

Figure 18. Chemiluminescent blotting with Biotin-TLS11a and testing of lysis buffers for Biotin-TLS11a pull-downs in MEAR cells. Pull downs were performed in a set of lysis buffers with varying compositions of detergents to optimize for protein extraction. APLB indicates the initial lysis buffer used for pilot pull-downs, while LB1-3 indicate detergent modifications to this buffer. In, input; PD, pull-down.

The two prominent signals from the blot in Figure 18 were analyzed using densitometry (Figure 19) in ImageJ to determine which lysis buffer yielded the highest signal.

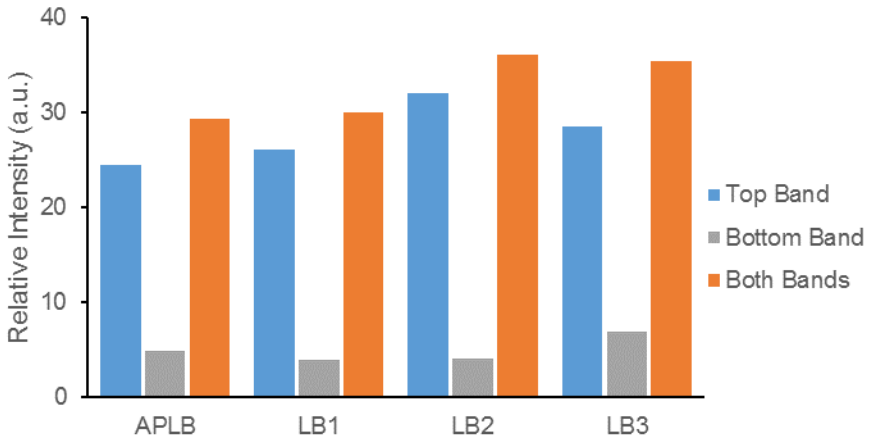

Figure 19. Densitometry analysis of bands in Biotin-TLS11a pull-downs. Lysis buffer 2 (LB2) resulted in the highest overall signal in Biotin-TLS11a blots. Top band, 114 kDa; bottom band, 72 kDa, corresponding to Figure 18.

The most intense signal as determined by densitometry indicated the best cell lysis of the buffers tested. The same samples were probed with actin antibody (Figure 20) for protein extraction and loading control in addition to Ponceau stain.

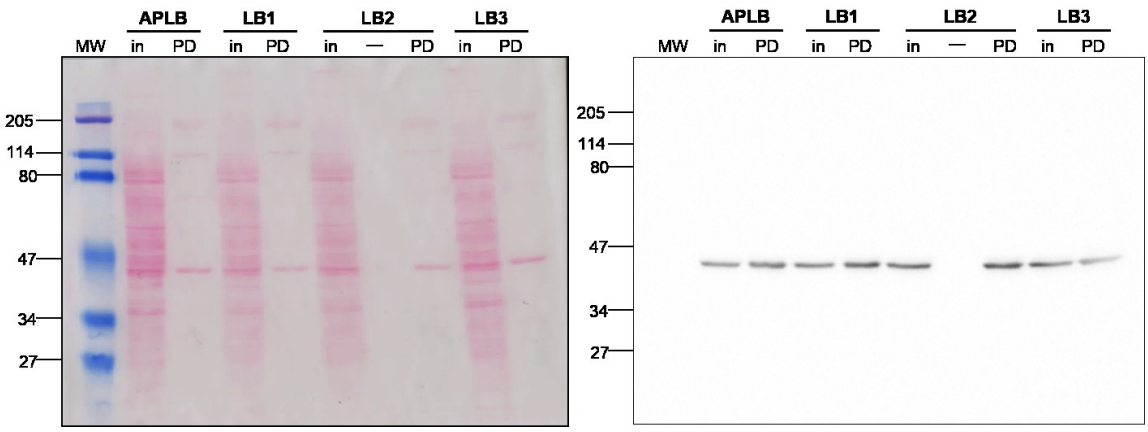

Figure 20. Western blot for actin from Biotin-TLS11a pull-downs done during lysis buffer optimization. The lane marked --- was skipped due to a deformation in the well of the SDS-PAGE gel. In, input; PD, pull-down.

Although the results of these experiments differed significantly from the patterns seen in prior fluorescent blotting, and no bands of similar molecular weight were detectable in the inputs, subsequent experiments were carried out and optimized with the detergent composition of LB2 nonetheless.

In the event that protein extraction, SDS-PAGE, and blotting methods denatured the TLS11a target to the extent that it became undetectable with aptamer blotting, it was hypothesized that labeling whole, live cells with TLS11a prior to cell lysis might help retain the aptamer-target interaction and improve signal. Refinement of techniques and longer exposures of the Biotin-TLS11a aptamer blots ultimately yielded results in which a band of ~114 kDa was visible in both the input and the pull-down. Encouragingly, a

high MW band near the 205 kDa marker was also visible in the pull-down.

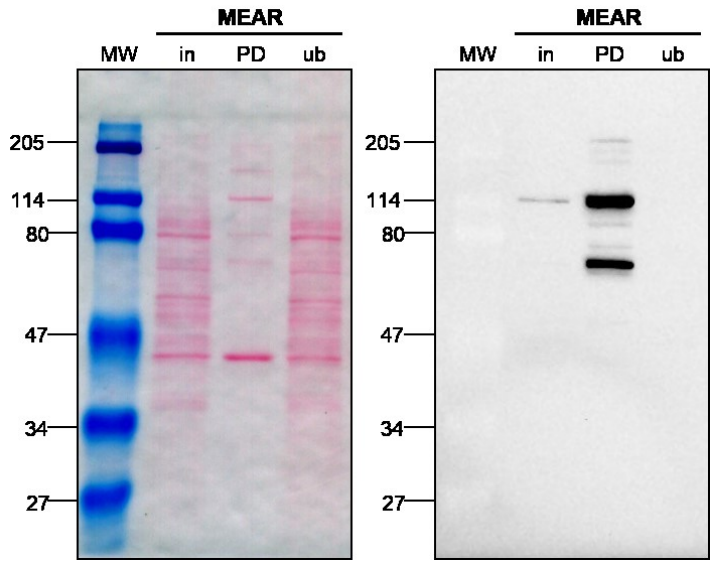

Figure 21. Optimized pull-down and blotting with Biotin-TLS11a. Improved signal to noise ratio was achieved in longer exposures of chemiluminescent blots, enabling detection of a target band in the input fraction.

However, due to the differences in data obtained thus far, it was hypothesized that a dual-labeled aptamer harboring both a fluorophore and an affinity tag might clarify the apparent conflicts by allowing for fluorescence detection in gels prior to blotting. Having TLS11a-Fluor on hand, a viable route to testing this idea was possible with existing reagents in the lab. EZ-Link NHS-LC-Biotin was used to biotinylate TLS11a-Fluor and TD05-Fluor. The biotinylated aptamers were then analyzed on a 20% TBE PAGE gel.

Shifts in apparent molecular weight of the biotinylated aptamers were noticeable for both aptamers upon fluorescence scan. After staining with GelRed, bands were more diffuse, and Biotin-TLS11a became visible. TD05 was barely perceptible after GelRed staining, although this may be attributable to its secondary structure, of which only half is base-paired (Figure 33) given that GelRed preferentially stains double-stranded DNA

over single stranded DNA.

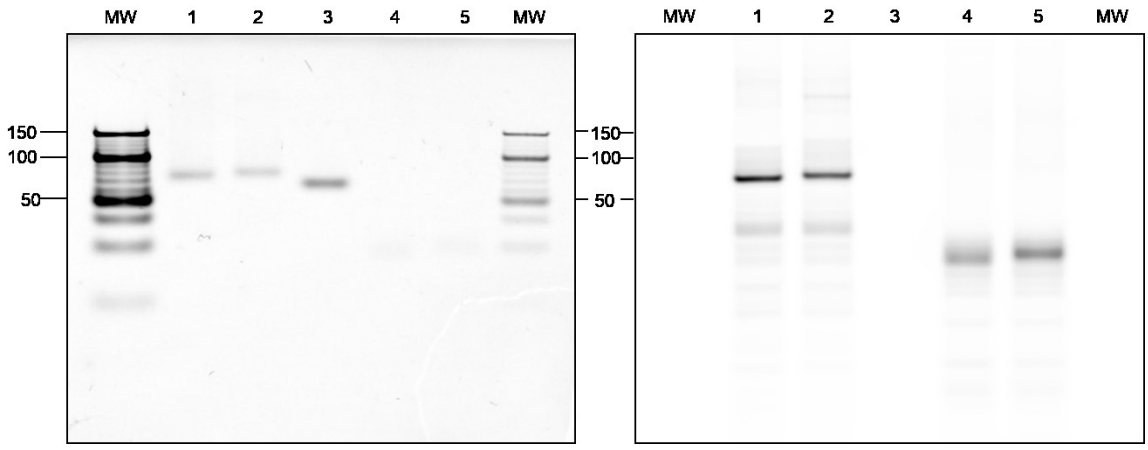

Figure 22. Biotinylated TLS11a-Fluor and TD05-Fluor. Aptamers were biotinylated and run on a 20% TBE PAGE gel. Right panel: gel immediately scanned for fluorescence. Left panel: the same gel imaged after staining overnight in GelRed. The MW lanes indicate 10bp O'Range Ruler DNA ladder at high load (left) and low load (right), respectively. Numbered lanes were loaded as follows: 1) TLS11a-Fluor, 2) biotinylated TLS11a-Fluor, 3) Biotin-TLS11a, 4) TD05-Fluor, 5) biotinylated TD05-Fluor.

While these results showed successful biotinylation of the aptamers, the fluorescence scan (Figure 22, right panel) displayed a significant number of species in addition to the predominant band prior to biotinylation. This may be due to degradation products containing the fluorophore, the formation of alternate structures in the absence of divalent cations in TBE, or the presence of alternate oligonucleotide products from synthesis that were not efficiently separated during HPLC purification. Intense adjustment of the fluorescence image in ImageJ (not shown) displayed the extent of alternate species present, which raised some concern regarding the integrity of the batch of TLS11a-Fluor in hands.

It was rationalized that in purchasing a new batch of aptamer, the use of dual labeled TLS11a would enable fluorescence detection simultaneously with affinity

purification. A desthiobiotin affinity tag was chosen instead of biotin because the streptavidin-desthiobiotin interaction is not as strong, allowing for elution from streptavidin with free biotin competition, a consideration for future planned mass spectrometry experiments.[61]

The use of this dual-modified aptamer enabled visualization of labeled cells prior to lysis and affinity purification. Formaldehyde was used to crosslink aptamer bound at the surface of the cells, covalently capturing target binding. MDA-MB-231 cells were used as an additional control, as they were unlikely to be detected by TLS11a. As expected, the CL.2 and MDA-MB-231 cells exhibited virtually no detectable fluorescence in the green channel with or without crosslinking (Figure 23 and Figure 24), while the MEAR cells exhibited stronger green fluorescence with crosslinking than without (Figure 25).

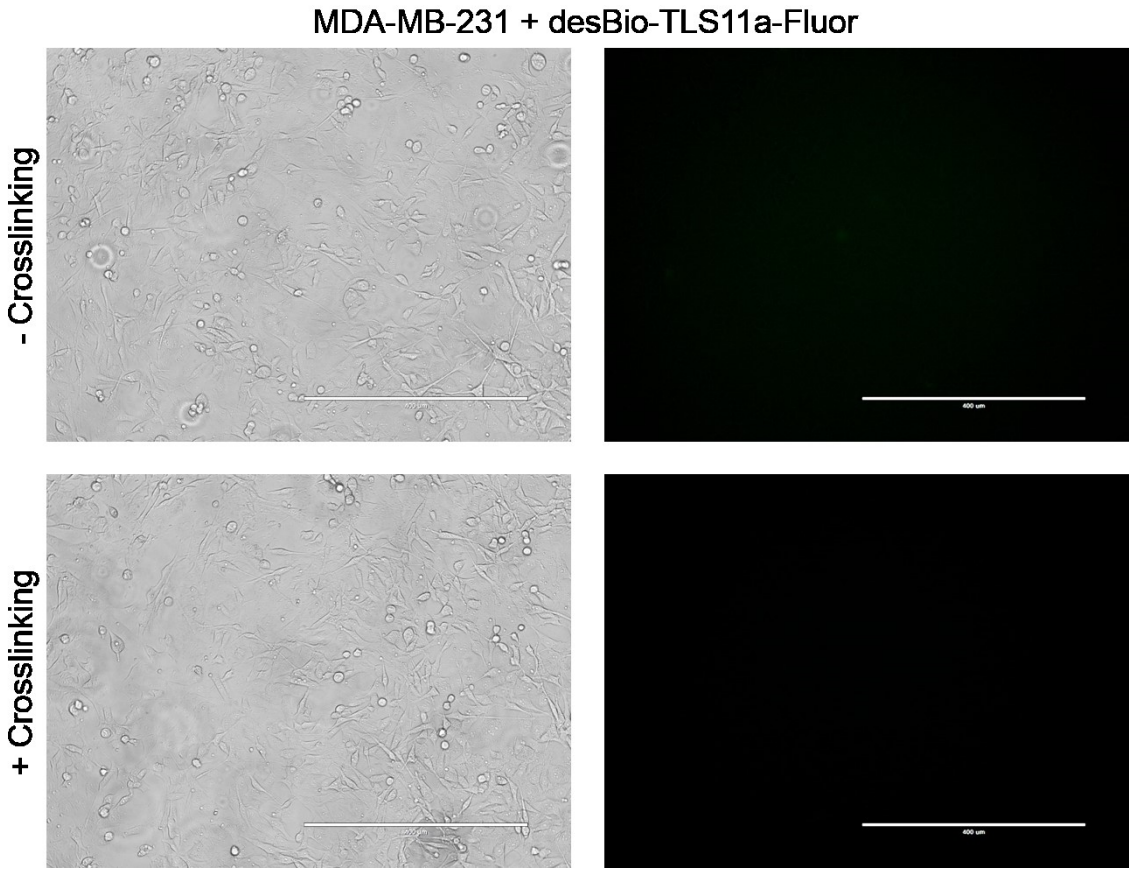

Figure 23. MDA-MB-231 cells labeled with desBio-TLS11a-Fluor with and without crosslinking. Images of cells prior to lysis at 10× magnification. Transmitted light (left) and green channel (right). Scale bars represent 400 μm.

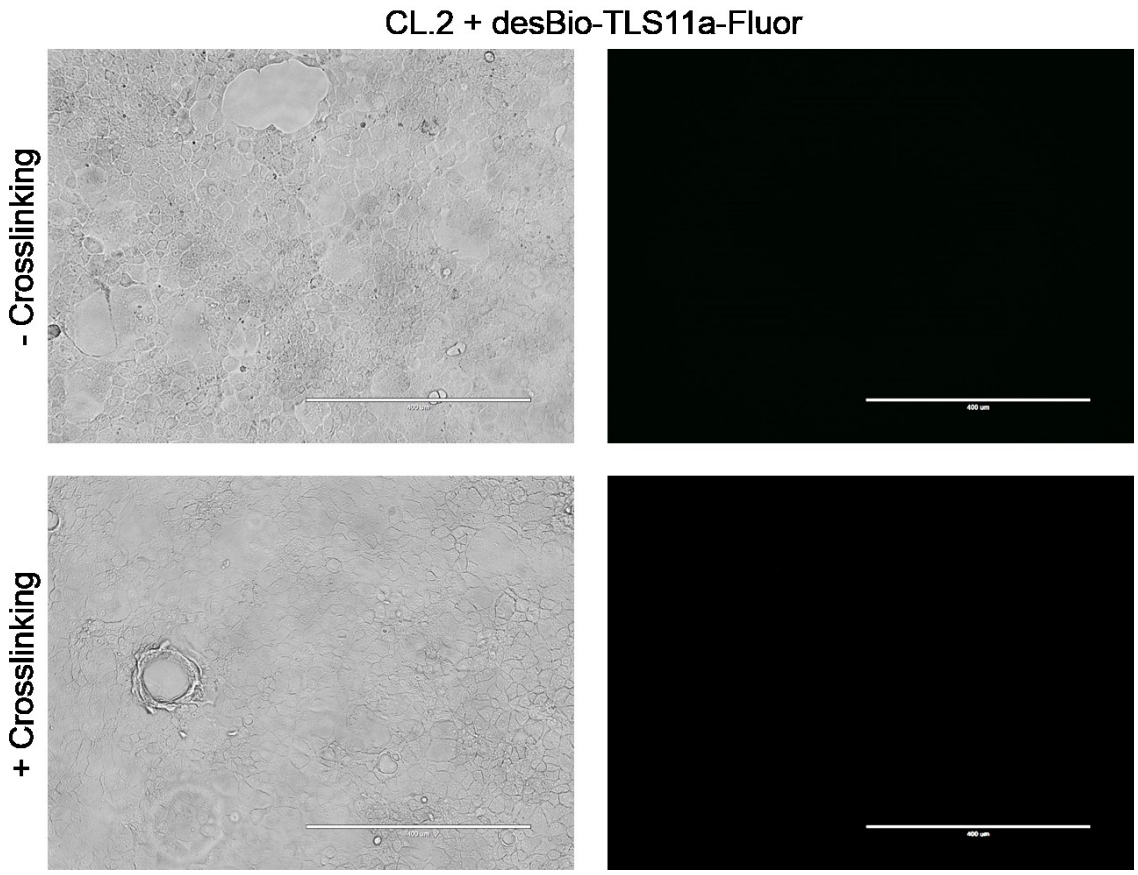

Figure 24. CL.2 cells labeled with desBio-TLS11a-Fluor with and without crosslinking. Images of cells prior to lysis at 10× magnification. Transmitted light (left) and green channel (right). Scale bars represent 400 µm.

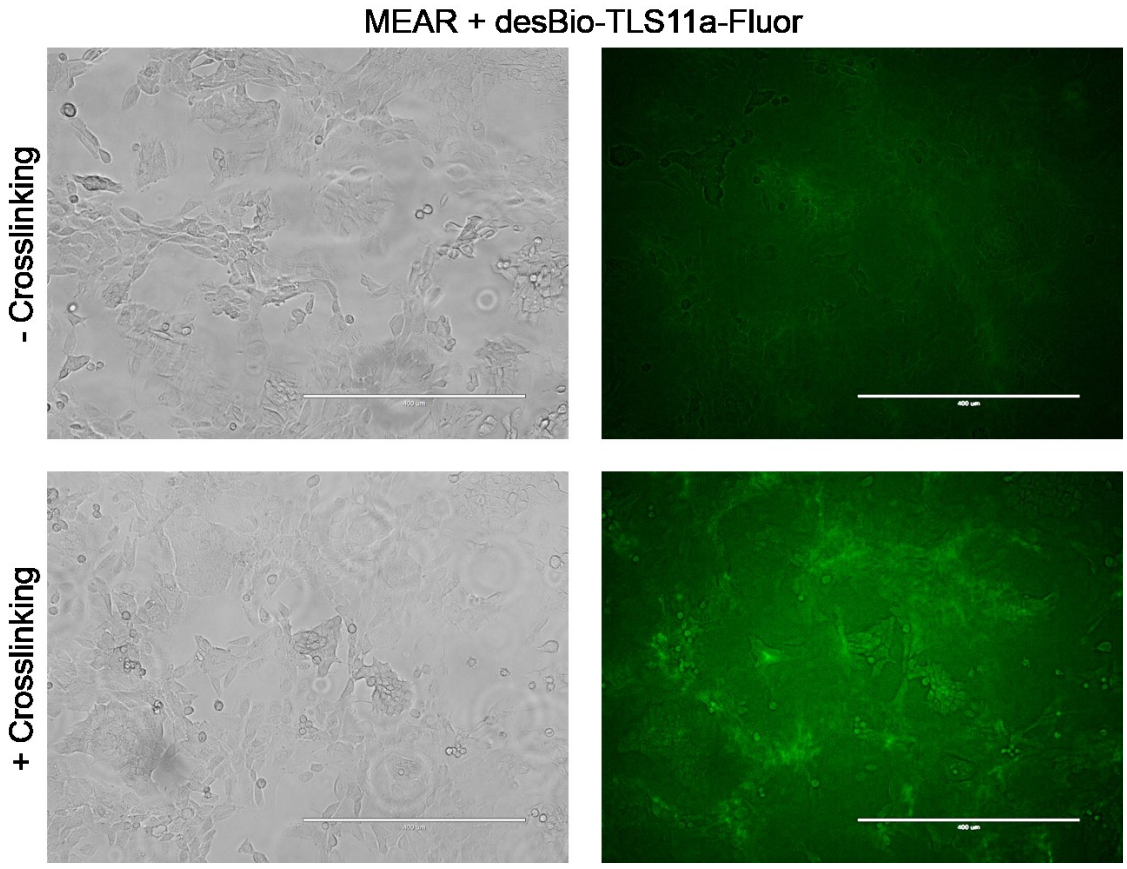

Figure 25. MEAR cells labeled with desBio-TLS11a-Fluor with and without crosslinking. Images of cells prior to lysis at 10× magnification. Transmitted light (left) and green channel (right). Scale bars represent 400 μm.

Cells appeared healthy and intact after staining or mock procedures, without signs of distress (rounding, detachment, blebbing, or ruffling). Transmitted light images of mock-treated cells (not shown) displayed identical quality of cell monolayers prior to harvest.

The labeled cells in Figure 23, Figure 24, and Figure 25 were harvested and subjected to pull-down experiments. The inputs and pull-down eluates were run on a 1.5 mm 15-well 10% SDS-PAGE gel, which was scanned for in-gel detection of fluorescent bands (Figure 26). The majority of the fluorescent signal appeared at the bottom of the

gel, although one high MW band of ~180 kDa was noticeable in the uncrosslinked MEAR pull-down lane upon adjustment of image brightness/contrast. This finding was in contrast with the expected appearance of a stronger specific signal at a similarly high MW in the crosslinked MEAR pull-down lane.

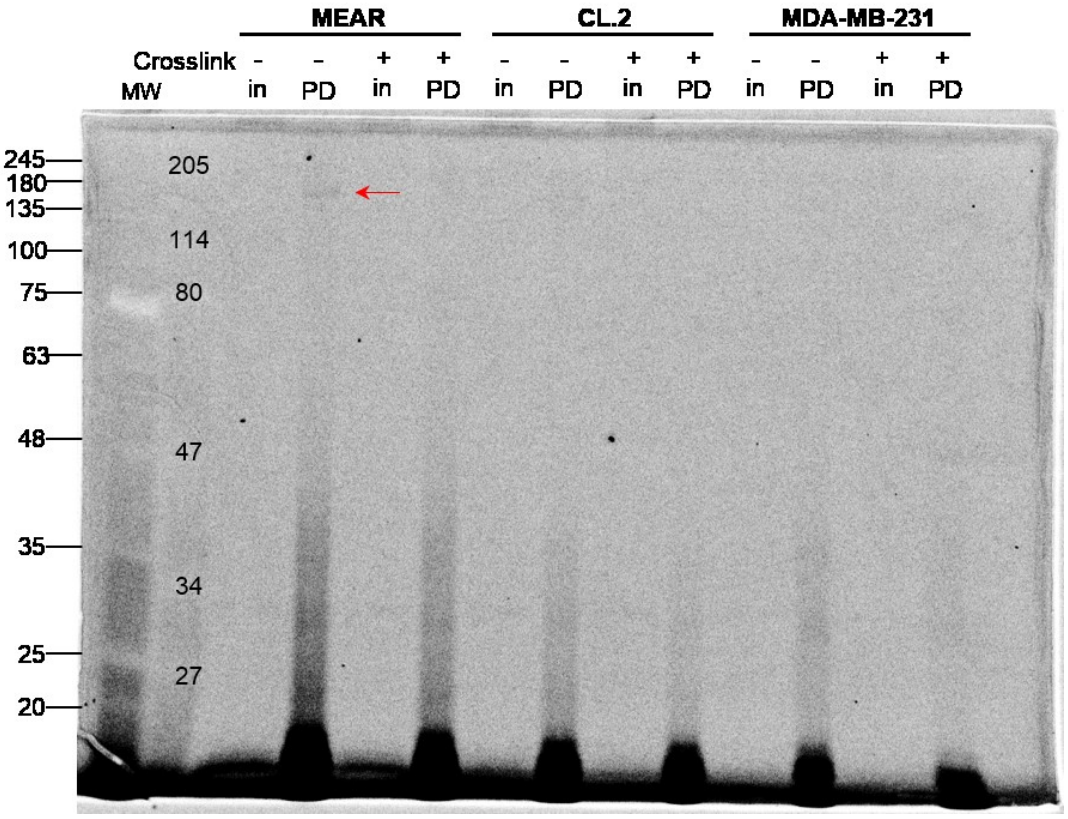

Figure 26. Fluorescence scan of gel containing desBio-TLS11a-Fluor labeled MEAR, CL.2, and MDA-MB-231 pull-downs with and without crosslinking. MW indicates Prism Ultra Protein Ladder. The MWs of the Broad Range protein standard (Bio-Rad) are marked in the following lane. Arrow indicates signal specific to the non-crosslinked MEAR PD lane which was not visible in any of the other lanes. In, input; PD, pull-down.

The gel shown in Figure 26 was immediately stained with colloidal Coomassie after scanning to assess relative loading of each sample and the distribution of total protein between crosslinked and non-crosslinked samples (Figure 27). Unexpectedly, a

larger number of protein bands were visible in the lanes containing samples that has not been crosslinked versus samples that had been crosslinked. As formaldehyde crosslinking captures protein-protein interactions, it was hypothesized that the crosslinked samples would display a wider array of proteins. Notably, the MDA-MB-231 samples produced very few bands in both conditions, consistent with lack of TLS11a binding (Figure 23). However, the abundance of proteins in the non-crosslinked CL.2 pull-down is not consistent with TLS11a binding determined by microscopy. This could be due, in part, to the higher amount of total protein present in this pull-down, as shown by intensity of staining of the input.

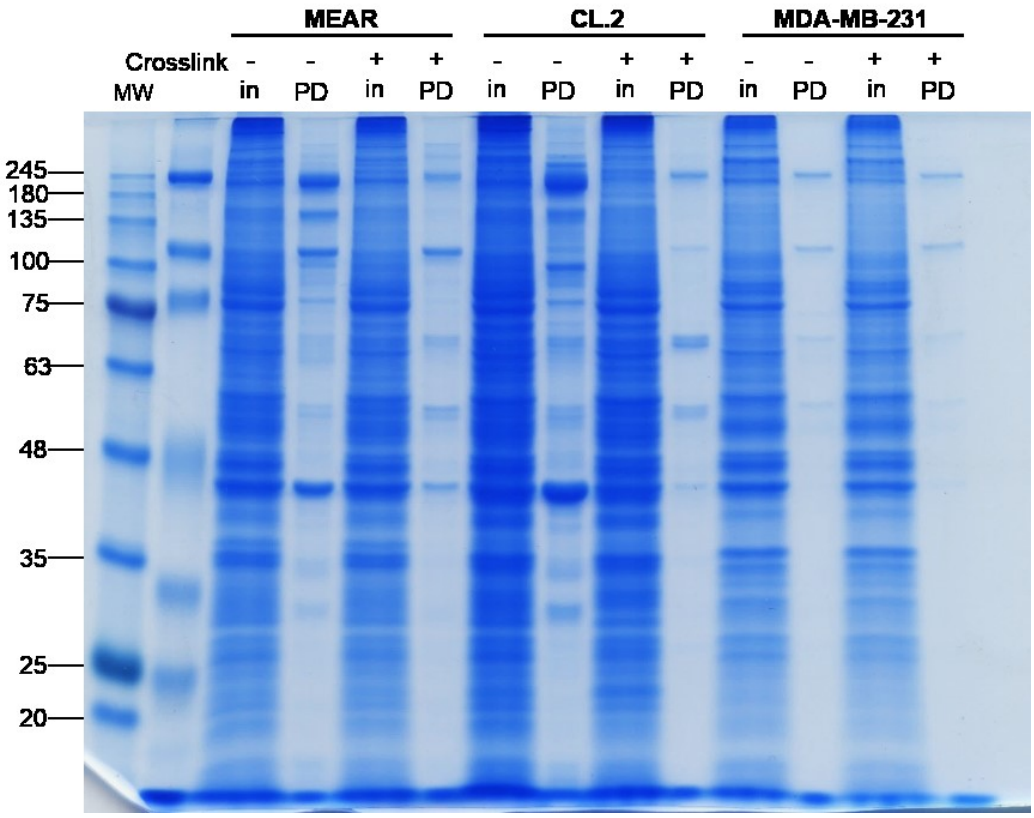

Figure 27. Colloidal stain of desBio-TLS11a-Fluor labeled MEAR, CL.2, and MDA-MB-231 pull-downs with and without crosslinking. The gel imaged in Figure 24 was stained with colloidal immediately after scanning. MW indicated on the left is Prism Ultra Protein Ladder; the next lane is the Broad Range protein standard from Bio-Rad. In, input; PD, pull-down.

To better resolve the fluorescent signal that appeared at the bottom of the gel in Figure 26, the same labeled samples, along with their corresponding unbound fractions, were run on 1 mm 10-well 12% gels (Figure 28).

The panels in Figure 28 are aligned to relay both relative loading and, in (B) and (D), representation of entire gels. No signals were visible in the bottom portions of the Biotin-TLS11a blots, or the top portions of the fluorescence gel scans. The banding patterns between crosslinked and non-crosslinked samples were very similar, with slight variations in intensity. The notable difference was the presence of very high MW bands (>245 kDa) in the Biotin-TLS11a blots, which were clearly visible in the non-crosslinked samples, and extremely faint in the crosslinked samples. Given that these bands were present in the input and unbound fractions, but not the pull-downs, indicates that they were non-specific.

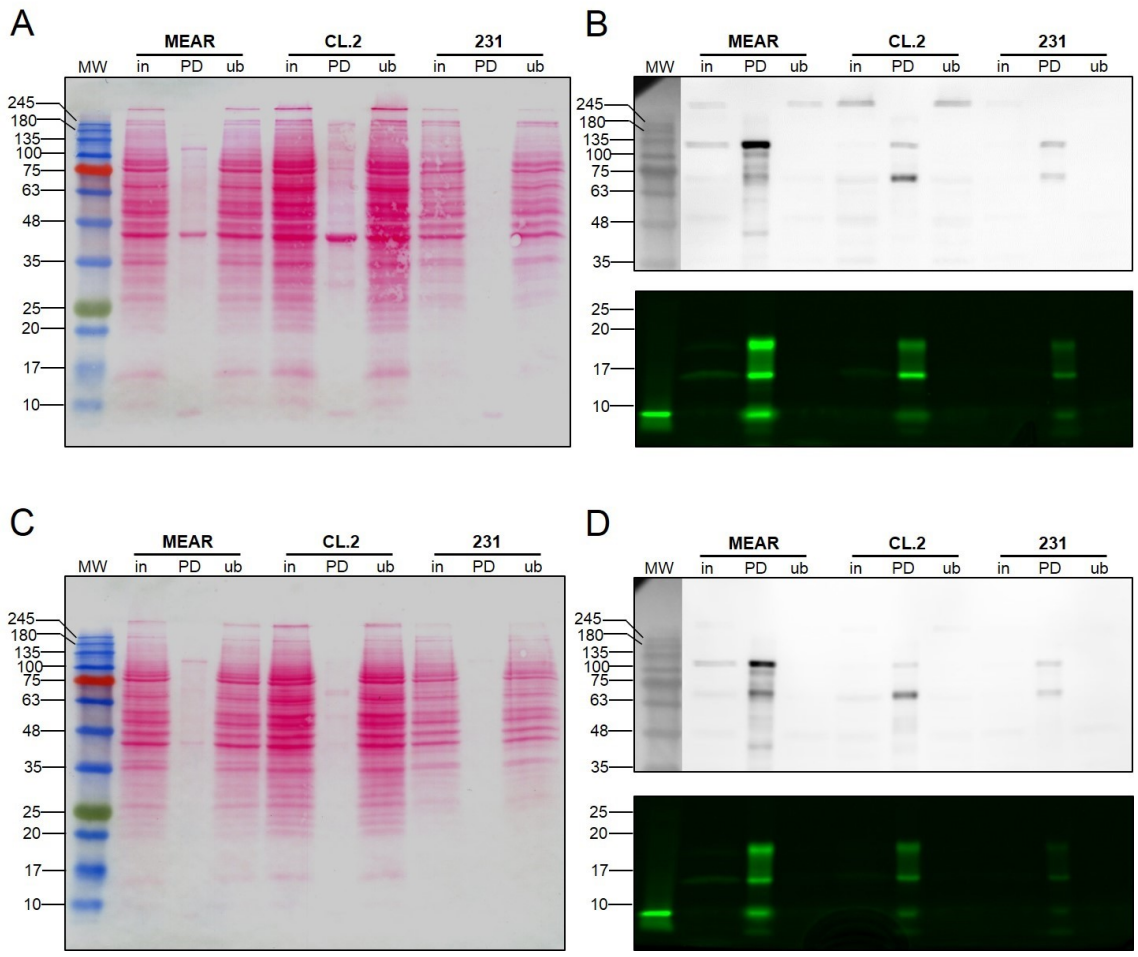

Figure 28. Biotin-TLS11a blots and fluorescent gel scans of desBio-TLS11a-Fluor labeled samples with and without crosslinking. (A) Ponceau stain and (B) Biotin-TLS11a blot (top), with fluorescent gel image (bottom) of non-crosslinked samples. (C) Ponceau stain and (D) Biotin-TLS11a blot (top), with fluorescent gel image (bottom) of crosslinked samples. Bottom panels of (B) and (D) are shown in false color using the green LUT from Image J. MW, molecular weight; in, input; PD, pull-down, ub, unbound.

The lack of signals overlapping between blotting and fluorescence gel scans could be due to several factors. DNA denatures at 95 °C, thus heating of TLS11a-target bound streptavidin beads in SDS sample buffer for 5 minutes would liberate the target molecule from TLS11a. Upon cooling after denaturation aptamers refold, however SDS can disrupt protein-DNA complexes.[76] This alone does not explain the similar patterns observed in formaldehyde treated samples, where interactions were covalently captured by

crosslinking.

Duplicate gels were run again, and blotted with anti-actin antibody (Figure 29). In the crosslinked samples, actin was extremely faint in the MEAR pull-down, but did not appear in pull-downs from the other cells. Initially, it was hypothesized that the TLS11a target protein interacted with actin based on results of early blots. Taking into account the differences in protein loading between the MEAR and CL.2 samples, the faint but detectable presence of actin in the crosslinked MEAR pull-down lends some support to this idea. Formaldehyde-captured actin would be released under conditions used for sample elution and SDS-PAGE. Absence of actin in the other crosslinked pull-downs also promotes this idea. If lack of actin signal were due exclusively to protein-protein crosslinking, leading to a shift in apparent molecular weight and/or destruction of the epitope recognized by the actin antibody, actin signal should be abrogated in all crosslinked samples, including input and unbound fractions.

In the absence of crosslinking in TLS11a labeled cells, actin was prominent in all but the MDA-MB-231 pull-down. This result is difficult to interpret, but may be due to promiscuity of non-specific protein interactions occurring after cell lysis and incubation with streptavidin beads.

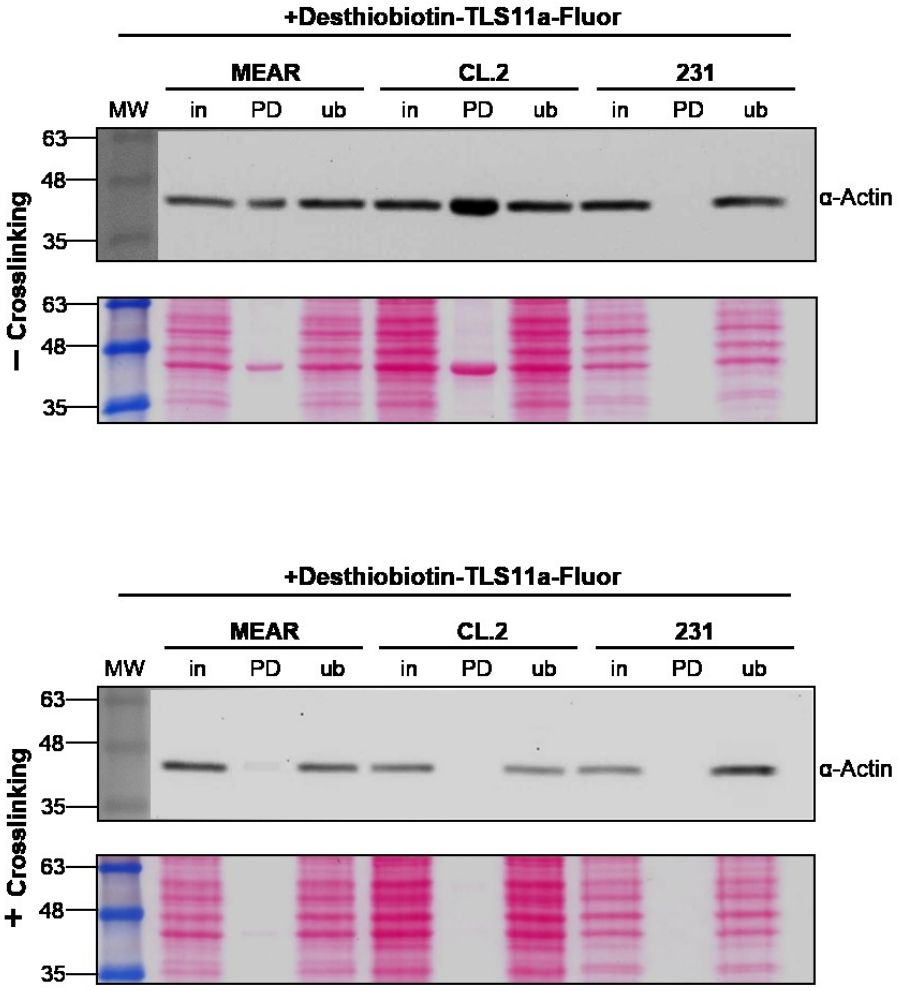

Figure 29. Actin blots of desBio-TLS11a-Fluor pull-downs with and without crosslinking. MW, molecular weight; in, input; PD, pull-down; ub, unbound.

A control experiment was done in which cells were treated in an identical manner to labeling, except no aptamer was present to determine the extent of non-specific binding (Figure 30). The input and pull-down fractions were run on a 12% SDS-PAGE gel, which was stained with colloidal Coomassie. These controls showed that a fairly high amount of non-specific binding occurred during incubation of unlabeled cell lysates with streptavidin dynabeads. MDA-MB-231 cells exhibited a significant amount of non-specific binding in the absence of both aptamer and crosslinking. Bands that appeared in

pull-downs from both labeled and control experiments were those at ~245 kDa, ~114 kDa, ~72 kDa, and the 43 kDa band corresponding to actin.

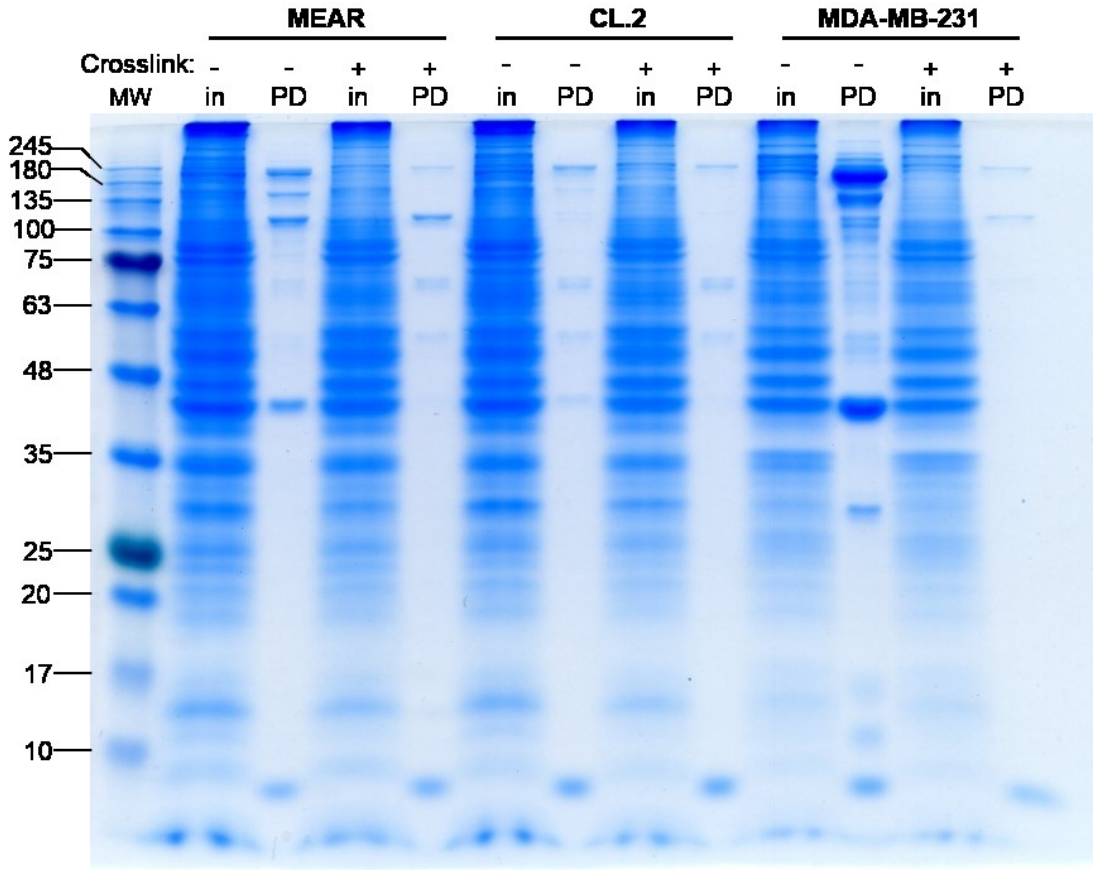

Figure 30. Colloidal stain of no-aptamer control MEAR, CL.2, and MDA-MB-231 pull-downs with and without crosslinking. Cells were incubated with media only (no aptamer) and subjected to the same procedure as in labeling as a control and run on a 1.5 mM 12% SDS-PAGE gel. MW, molecular weight; in, input; PD, pull-down; ub, unbound.

To determine if these proteins were similar to or the same as the proteins detected in the aptamer labeled cells, Biotin-TLS11a (Figure 31) blots and actin blots (Figure 32) were performed for comparison. The banding patterns in control Biotin-TLS11a blots were similar to those in labeled cells. Given the enrichment of signal in the pull-down fractions, this may indicate that signal in these blots could be due to NeutrAvidin-HRP

recognition of biotinylated proteins instead of specific Biotin-TLS11a mediated recognition.

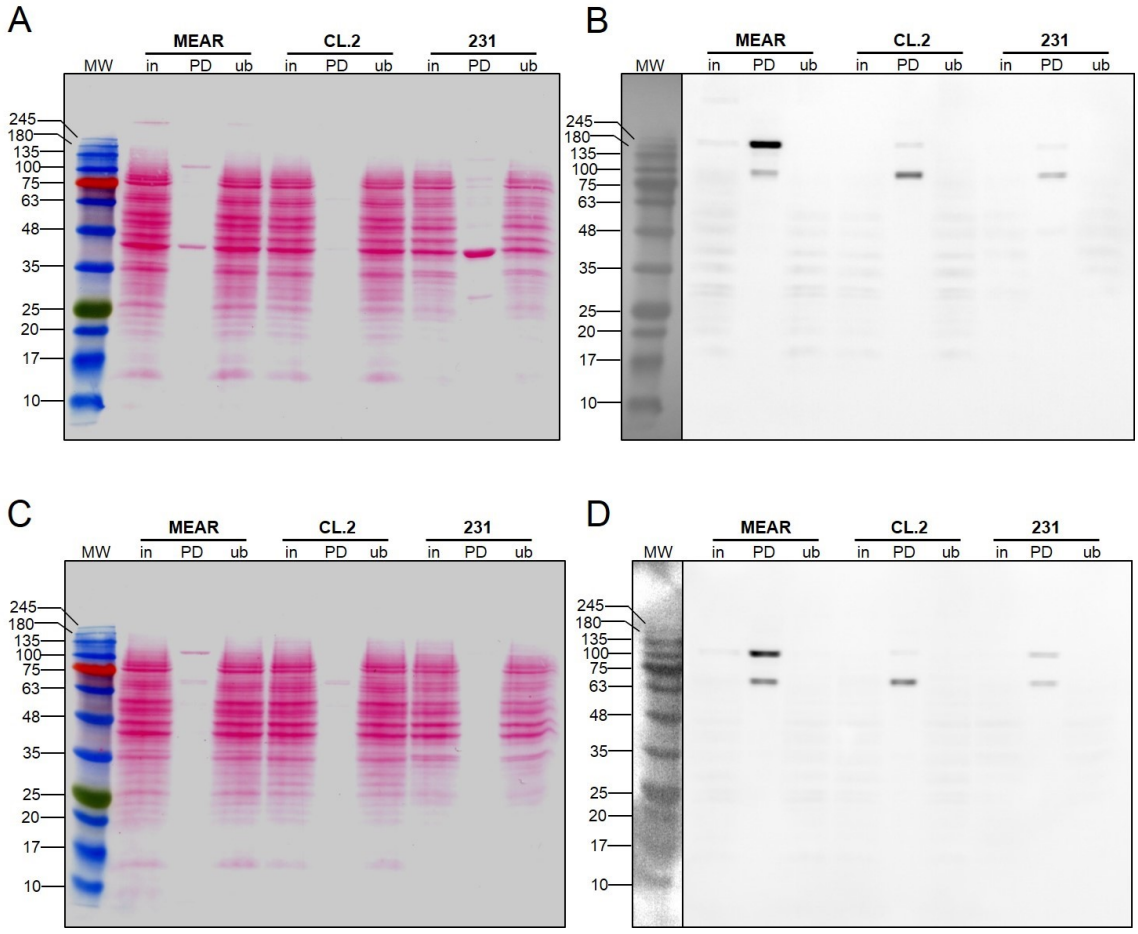

Figure 31. Biotin-TLS11a blots of no-aptamer control pull-downs with and without crosslinking. (A and B) Ponceau stained membrane and Biotin-TLS11a blot, respectively, of non-crosslinked samples. (C and D) Ponceau stained membrane and Biotin-TLS11a blot of crosslinked samples, respectively. MW, molecular weight; in, input; PD, pull-down; ub, unbound.

Endogenously biotinylated carboxylases are present in mammalian cell cytosol and mitochondria.[77,78] Acetyl coA carboxylase, pyruvate carboxylase, 3-methylcrotonyl coA carboxylase, and propionyl coA carboxylase, all of which are endogenously biotinylated, have reported molecular weights of 220 kDa, 130 kDa, 75 kDa, and 72 kDa, respectively. These proteins have been reported as non-specific background in

biotinylated aptamer purifications[45] (supporting information). The molecular weights of these proteins coincide relatively well with the signals observed in Biotin-TLS11a blotting.

Blotting for actin in the control treatments without aptamer showed a similar pattern to what was observed in labeled cells. However, the most important difference to note in the control blots is the absence of any detectable actin in the crosslinked MEAR pull-down. Overall, the actin signals were weaker in these samples, with the exception of MDA-MB-231 cells.

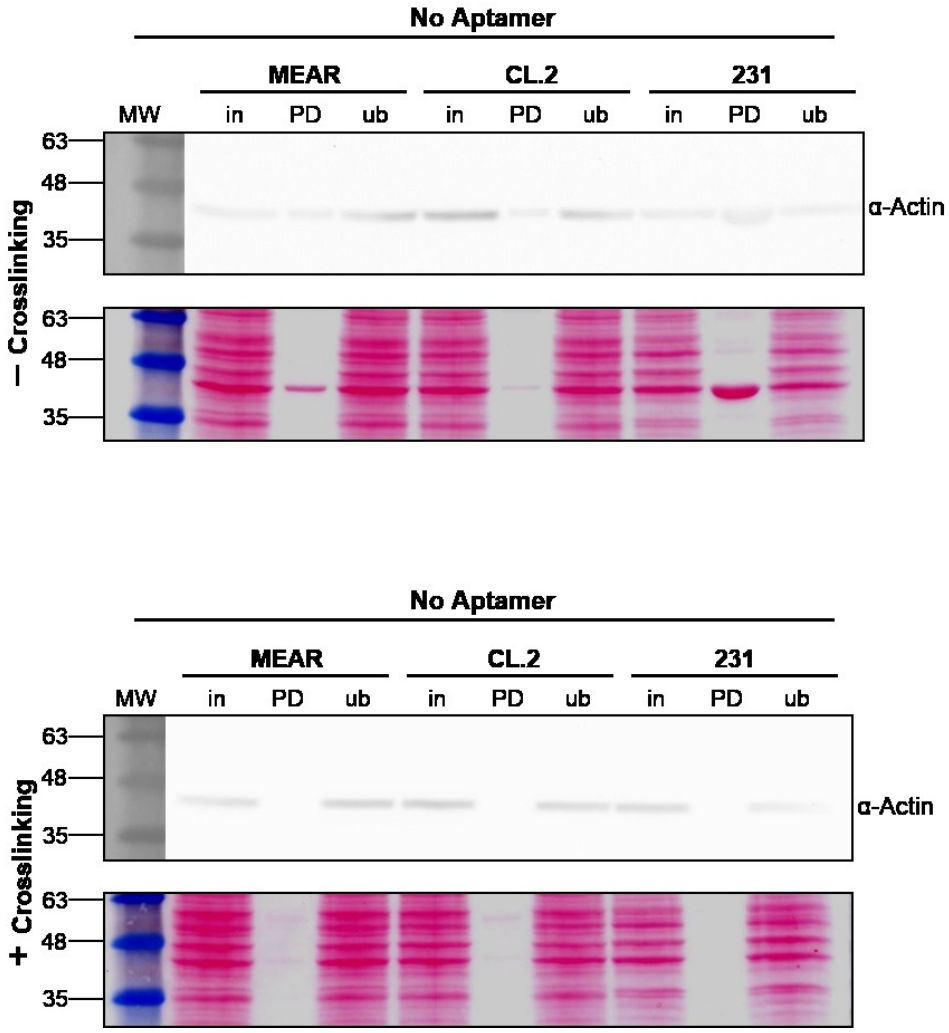

Figure 32. Actin blots of no-aptamer control pull-downs with and without crosslinking. MW, molecular weight; in, input; PD, pull-down; ub, unbound.

The variability of actin in the presence or absence of TLS11a in all samples tested could be due to a variety of factors, however direct investigation of these particular observations is beyond the present scope of this work. It has been reported that streptavidin has a three-peptide RYD sequence that can act as a recognition site for the RGD receptor of fibronectin.[79] Actin and fibronectin associate strongly in the extracellular matrix of cells in culture.[80] It seems possible that this may be the source of non-specific actin signals detected in this work. The absence of actin bands in both

labeled and control crosslinked samples could be due to protein crosslinking of actin to fibronectin, shifting its apparent molecular weight and leading to loss of signal in the pull-down fractions.

4. SUMMARY AND CONCLUSIONS

TLS11a-functionalized biodegradable nanoparticles displayed equivalent efficacy to that of doxorubicin alone, and the nanoparticles themselves did not cause cytotoxicity to cells in culture. While normal hepatocyte cells were also affected by the drug loaded NPs, this is explainable in context of the fundamental mechanism by which these nanocarriers release their drug payload into the local environment. These results indicate that testing of this targeted drug delivery system *in vivo* may exhibit good efficacy in HCC treatment models.

The affinity purification of TLS11a target complexes in this work represents the preliminary optimization steps required for obtaining a more definitive indication of what a specific TLS11a target protein might be. The methods used here demonstrate how confounding non-specific binding can be, even with the use of seemingly specific affinity tools. The presence of several prominent endogenously biotinylated proteins in mammalian cells and the apparent promiscuity of streptavidin protein-binding are critical factors to consider when designing controls for such experiments.

The recommended methods for releasing biotinylated ligands from streptavidin-conjugated supports is another issue that warrants a cautious approach. Manufacturers' instructions typically involve the use of heat to liberate biotin from streptavidin, with higher temperatures yielding better results in terms of sample yield. Boiling of beads in reducing sample buffer is a common method of recovering captured samples. However, these conditions appear to increase background contaminants by releasing proteins non-specifically bound to streptavidin by protein-protein interaction. Furthermore, when used

with formaldehyde crosslinking, this strategy must be methodically analyzed to determine if heat will affect desired results. Formaldehyde crosslinks are reversible, and high heat under denaturing conditions can cause reversal of these cross-links [81]. The heat and denaturing conditions used in experiments presented in this work likely explain, in part, lack of specific TLS11a-specific signals. Additionally, the claim that cell-SELEX evolved aptamers may recognize proteins in relatively low abundance, increasing the amount of starting material/cells and decreasing non-specific binding, are potentially critical to the success of further experiments.

In light of these results, plans for future experiments include eluting desthiobiotin-TLS11a-target complexes with a solution containing free biotin, as competitive ligand elution should produce cleaner eluates than boiling. Given the high expression of biotinylated carboxylases in liver-derived cells, whole-cell labeling may need to be tested against TLS11a-target binding *in vitro* that includes a pre-clearing step where unlabeled cell lysates are incubated with streptavidin resin; endogenously biotinylated proteins and those that bind to streptavidin via direct protein interaction (non-biotin mediated) can thus be removed and discarded prior to incubation with aptamer. An additional factor that can be considered is the use of bead-washing buffers that include progressively increasing salt concentrations with formaldehyde-crosslinked samples, as high salt conditions disrupt many non-covalent interactions in protein-protein interactions. These are common steps in widely employed immunoprecipitation experiments where protein-DNA interactions are examined. Thus, there is a well-established knowledge base to draw from in refining subsequent procedures.

The future directions for this work include steps outlined above and subsequent

submission of samples for mass spectrometry analysis to gain a data set from which a putative TLS11a target could be verified. The work presented here has laid the groundwork for avoiding artefacts in experimental procedures involving affinity purification with biotinylated aptamers.

APPENDIX SECTION

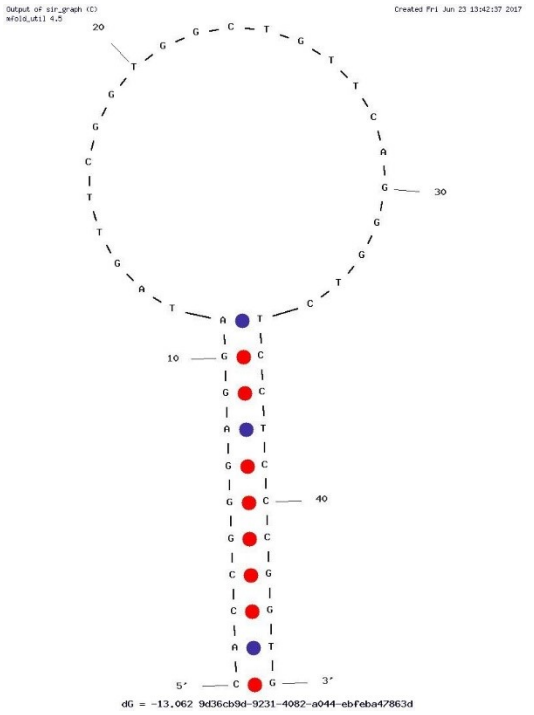

Figure 33. Predicted secondary structure of non-targeting aptamer TD05. The UNAfold tool from IDT was used to predict the secondary structure of TD05 and generate an image.

Table 8. List and compositions of buffers and reagents not previously specified.

Solution	Reagent	Concentration	pH	Sterilization	Storage
PMSF	PMSF Isopropanol	200 mM solvent	n/a	n/a	-20 °C
TBE	Tris base Boric acid EDTA	100 mM 100 mM 2 mM	Not adjusted	None	RT
1 M Tris-HCl	Tris base	1 M	6.8 with HCl	0.2 µm filtered	RT
1.5 M Tris-HCl	Tris base	1 M	8.8 with HCl	0.2 µm filtered	RT
1 M HEPES	HEPES	1 M	7.9 with NaOH	0.2 µm filtered	4 °C

REFERENCES

(1) Siegel, R., Miller, K., and Jemal, A. (2017) Cancer statistics, 2017. *CA Cancer J. Clin. 67*, 7–30.

(2) Knox, J. J., Cleary, S. P., and Dawson, L. A. (2015) Localized and systemic approaches to treating hepatocellular carcinoma. *J. Clin. Oncol. 33*, 1835–44.

(3) Ferlay, J., Soerjomataram, I., Dikshit, R., Eser, S., Mathers, C., Rebelo, M., Parkin, D. M., Forman, D., and Bray, F. (2015) Cancer incidence and mortality worldwide: Sources, methods and major patterns in GLOBOCAN 2012. *Int. J. Cancer 136*, E359–E386.

(4) American Cancer Society. (2017) Cancer Facts & Figures 2017. Atlanta.

(5) Forner, A., Llovet, J. M., and Bruix, J. (2012) Hepatocellular carcinoma. *Lancet 379*, 1245–1255.

(6) Jelic, S., and Sotiropoulos, G. C. (2010) Hepatocellular carcinoma: ESMO Clinical Practice Guidelines for diagnosis, treatment and follow-up. *Ann. Oncol. 21*, v59–v64.

(7) Bruix, J., and Sherman, M. (2005) Management of hepatocellular carcinoma. *Hepatology 42*, 1208–1236.

(8) Daniele, G., Costa, N., Lorusso, V., Costa-Maia, J., Pache, I., and Pirisi, M. (2013) Methodological assessment of HCC literature. *Ann. Oncol. 24*, ii6-ii14.

(9) Attwa, M. H. (2015) Guide for diagnosis and treatment of hepatocellular carcinoma. *World J. Hepatol. 7*, 1632.

(10) Llovet, J. M., Ricci, S., Mazzaferro, V., Hilgard, P., Gane, E., Blanc, J. J. J., de Oliveira, A. A. C. A., Santoro, A., Raoul, J.-L. J., Forner, A., Schwartz, M., Porta, C., Zeuzem, S., Bolondi, L., Greten, T. T. F. T., Galle, P. R. P., Seitz, J.-F. J., Borbath, I., Häussinger, D., Giannaris, T., Shan, M., Moscovici, M., Voliotis, D., Bruix, J., Group, S. I. S., Oliveira, A. C. De, Sc, B., and Ph, D. (2008) Sorafenib in advanced hepatocellular carcinoma. *N. Engl. J. Med. 359*, 378–390.

(11) Bruix, J., Takayama, T., Mazzaferro, V., Chau, G. Y., Yang, J., Kudo, M., Cai, J., Poon, R. T., Han, K. H., Tak, W. Y., Lee, H. C., Song, T., Roayaie, S., Bolondi, L., Lee, K. S., Makuuchi, M., Souza, F., Le Berre, M. A., Meinhardt, G., and Llovet, J. M. (2015) Adjuvant sorafenib for hepatocellular carcinoma after resection or ablation (STORM): A phase 3, randomised, double-blind, placebo-controlled trial. *Lancet Oncol. 16*, 1344–1354.

(12) Maeda, H., Wu, J., Sawa, T., Matsumura, Y., and Hori, K. (2000) Tumor vascular permeability and the EPR effect in macromolecular therapeutics: A review. *J. Controlled Release 65*, 271–284.

(13) Byrne, J. D., Betancourt, T., and Brannon-Peppas, L. (2008) Active targeting schemes for nanoparticle systems in cancer therapeutics. *Adv. Drug Delivery Rev. 60*, 1615–1626.

(14) Danhier, F., Feron, O., and Preat, V. (2010) To exploit the tumor microenvironment: Passive and active tumor targeting of nanocarriers for anti-cancer drug delivery. *J. Controlled Release 148*, 135–146.

(15) Kobayashi, H., Watanabe, R., and Choyke, P. L. (2014) Improving conventional enhanced permeability and retention (EPR) effects; What is the appropriate target? *Theranostics 4*, 81–89.

(16) Ventola, C. L., Bharali, D. J., and Mousa, S. A. (2010) The Nanomedicine Revolution: Part 1: Emerging Concepts. *P T. 128*, 512–525.
(17) Bobo, D., Robinson, K. J., Islam, J., Thurecht, K. J., and Corrie, S. R. (2016) Nanoparticle-Based Medicines: A Review of FDA-Approved Materials and Clinical Trials to Date. *Pharm. Res. 33*, 2373–2387.
(18) Ventola, C. L. (2012) The nanomedicine revolution: part 2: current and future clinical applications. *P T. 37*, 582–91.
(19) Masood, F. (2016) Polymeric nanoparticles for targeted drug delivery system for cancer therapy. *Mater. Sci. Eng. C 60*, 569–578.
(20) Kamaly, N., Xiao, Z., Valencia, P. M., Radovic-Moreno, A. F., and Farokhzad, O. C. (2012) Targeted polymeric therapeutic nanoparticles: design, development and clinical translation. *Chem. Soc. Rev. 41*, 2971–3010.
(21) Desai, N. (2012) Challenges in Development of Nanoparticle-Based Therapeutics. *AAPS J. 14*, 282–295.
(22) Peer, D., Karp, J. M., Hong, S., Farokhzad, O. C., Margalit, R., and Langer, R. (2007) Nanocarriers as an emerging platform for cancer therapy. *Nat. Nanotechnol. 2*, 751–760.
(23) Ellington, A. D., and Szostak, J. W. (1990) In vitro selection of RNA molecules that bind specific ligands. *Nature 346*, 818–822.
(24) Tuerk, C., and Gold, L. (1990) Systematic evolution of ligands by exponential enrichment: RNA ligands to bacteriophage T4 DNA polymerase. *Science 249*, 505–510.
(25) Gold, L., Ayers, D., Bertino, J., Bock, C., Bock, A., Brody, E. N., Carter, J., Dalby, A. B., Eaton, B. E., Fitzwater, T., Flather, D., Forbes, A., Foreman, T., Fowler, C., Gawande, B., Goss, M., Gunn, M., Gupta, S., Halladay, D., Heil, J., Heilig, J., Hicke, B., Husar, G., Janjic, N., Jarvis, T., Jennings, S., Katilius, E., Keeney, T. R., Kim, N., Koch, T. H., Kraemer, S., Kroiss, L., Le, N., Levine, D., Lindsey, W., Lollo, B., Mayfield, W., Mehan, M., Mehler, R., Nelson, S. K., Nelson, M., Nieuwlandt, D., Nikrad, M., Ochsner, U., Ostroff, R. M., Otis, M., Parker, T., Pietrasiewicz, S., Resnicow, D. I., Rohloff, J., Sanders, G., Sattin, S., Schneider, D., Singer, B., Stanton, M., Sterkel, A., Stewart, A., Stratford, S., Vaught, J. D., Vrkljan, M., Walker, J. J., Watrobka, M., Waugh, S., Weiss, A., Wilcox, S. K., Wolfson, A., Wolk, S. K., Zhang, C., and Zichi, D. (2010) Aptamer-Based Multiplexed Proteomic Technology for Biomarker Discovery. *PLoS One 5*, e15004.
(26) Keefe, A. D., Pai, S., and Ellington, A. (2010) Aptamers as therapeutics. *Nat. Rev. Drug Discovery 9*, 537–550.
(27) Radom, F., Jurek, P. M., Mazurek, M. P., Otlewski, J., and Jeleń, F. (2013) Aptamers: Molecules of great potential. *Biotechnol. Adv.*
(28) Ma, H., Liu, J., Ali, M. M., Mahmood, M. A. I., Labanieh, L., Lu, M., Iqbal, S. M., Zhang, Q., Zhao, W., and Wan, Y. (2015) Nucleic acid aptamers in cancer research, diagnosis and therapy. *Chem. Soc. Rev. 44*, 1240–1256.
(29) Sun, H., and Zu, Y. (2015) A Highlight of recent advances in aptamer technology and its application. *Molecules 20*, 11959–11980.

(30) Blackburn, M. G., Gait, M. J., Loakes, D., and Williams, D. M. (Eds.). (2006) Nucleic Acids in Chemistry and Biology 3rd ed. The Royal Society of Chemistry, Cambridge, UK.
(31) Rozenblum, G. T., Lopez, V. G., Vitullo, A. D., and Radrizzani, M. (2016) Aptamers: current challenges and future prospects. *Expert Opin. Drug Discov. 11*, 127–135.
(32) Walls, D., and Loughran, S. T. (2011) Protein Chromatography, in *Methods in molecular biology (Clifton, N.J.)*, pp 151–175.
(33) Song, K. M., Lee, S., and Ban, C. (2012) Aptamers and their biological applications. *Sensors 12*, 612–631.
(34) Zhu, Q., Liu, G., and Kai, M. (2015) DNA Aptamers in the Diagnosis and Treatment of Human Diseases. *Molecules 20*, 20979–97.
(35) Tan, S. Y., Acquah, C., Sidhu, A., Ongkudon, C. M., Yon, L. S., and Danquah, M. K. (2016) SELEX Modifications and Bioanalytical Techniques for Aptamer–Target Binding Characterization. *Crit. Rev. Anal. Chem. 46*, 521–537.
(36) Mallikaratchy, P. (2017) Evolution of complex target SELEX to identify aptamers against mammalian cell-surface antigens. *Molecules 22*, 1–12.
(37) Choi, S., and Ban, C. (2016) Crystal structure of a DNA aptamer bound to Pv LDH elucidates novel single-stranded DNA structural elements for folding and recognition. *Sci. Rep. 6*, 34998.
(38) Xiao, Z., Shangguan, D., Cao, Z., Fang, X., and Tan, W. (2008) Cell-specific internalization study of an aptamer from whole cell selection. *Chem. - Eur. J. 14*, 1769–1775.
(39) Daniels, D. a, Chen, H., Hicke, B. J., Swiderek, K. M., and Gold, L. (2003) A tenascin-C aptamer identified by tumor cell SELEX: systematic evolution of ligands by exponential enrichment. *Proc. Natl. Acad. Sci. U.S.A. 100*, 15416–15421.
(40) Shangguan, D., Li, Y., Tang, Z., Cao, Z. C., Chen, H. W., Mallikaratchy, P., Sefah, K., Yang, C. J., and Tan, W. (2006) Aptamers evolved from live cells as effective molecular probes for cancer study. *Proc. Natl. Acad. Sci. U.S.A. 103*, 11838–11843.
(41) Chen, M., Yu, Y., Jiang, F., Zhou, J., Li, Y., Liang, C., Dang, L., Lu, A., and Zhang, G. (2016) Development of cell-SELEX technology and its application in cancer diagnosis and therapy. *Int. J. Mol. Sci. 17*, 1–14.
(42) Sefah, K., Shangguan, D., Xiong, X., O'Donoghue, M. B., and Tan, W. (2010) Development of DNA aptamers using Cell-SELEX. *Nat. Protoc. 5*, 1169–1185.
(43) Meng, H. M., Fu, T., Zhang, X. B., and Tan, W. (2015) Cell-SELEX-based aptamer-conjugated nanomaterials for cancer diagnosis and therapy. *Natl. Sci. Rev. 2*, 71–84.
(44) Chang, Y. M., Donovan, M. J., and Tan, W. (2013) Using aptamers for cancer biomarker discovery. *J. Nucleic Acids 2013*, 817350.
(45) Bing, T., Shangguan, D., and Wang, Y. (2015) Facile Discovery of Cell-surface Protein Targets of Cancer Cell Aptamers. *Mol. Cell. Proteomics 14*, 2692–2700.
(46) Shangguan, D., Meng, L., Cao, Z. C., Xiao, Z., Fang, X., Li, Y., Cardona, D., Witek, R. P., Liu, C., and Tan, W. (2008) Identification of Liver Cancer-Specific Aptamers Using Whole Live Cells. *Anal. Chem. 80*, 721–728.

(47) Meng, L., Yang, L., Zhao, X., Zhang, L., Zhu, H., Liu, C., and Tan, W. (2012) Targeted Delivery of Chemotherapy Agents Using a Liver Cancer-Specific Aptamer. *PLoS One 7*, e33434.
(48) Weigum, S. E., Sutton, M., Barnes, E., Miller, S., and Betancourt, T. (2014) Targeting hepatocellular carcinoma with aptamer-functionalized PLGA/PLA-PEG nanoparticles. *Proc. SPIE 9166*, 916605–916610.
(49) Kashefi-Kheyrabadi, L., Mehrgardi, M. a, Wiechec, E., Turner, A. P. F., and Tiwari, A. (2014) Ultrasensitive detection of human liver hepatocellular carcinoma cells using a label-free aptasensor. *Anal. Chem. 86*, 4956–60.
(50) Qu, L., Xu, J., Tan, X., Liu, Z., Xu, L., and Peng, R. (2014) Dual-Aptamer Modification Generates a Unique Interface for Highly Sensitive and Specific Electrochemical Detection of Tumor Cells. *ACS Appl. Mater. Interfaces 6*, 7309–15.
(51) Sun, D., Lu, J., Chen, Z., Yu, Y., and Mo, M. (2015) A repeatable assembling and disassembling electrochemical aptamer cytosensor for ultrasensitive and highly selective detection of human liver cancer cells. *Anal. Chim. Acta 885*, 166–173.
(52) Sun, D., Lu, J., Zhong, Y., Yu, Y., Wang, Y., Zhang, B., and Chen, Z. (2016) Sensitive electrochemical aptamer cytosensor for highly specific detection of cancer cells based on the hybrid nanoelectrocatalysts and enzyme for signal amplification. *Biosens. Bioelectron. 75*, 301–307.
(53) Weigum, S., McIvor, E., Munoz, C., Feng, R., Cantu, T., Walsh, K., and Betancourt, T. (2016) Targeted therapy of hepatocellular carcinoma with aptamer-functionalized biodegradable nanoparticles. *J. Nanoparticle Res. 18*, 341.
(54) Zhang, D., Zheng, A., Li, J., Wu, M., Wu, L., Wei, Z., Liao, N., Zhang, X., Cai, Z., Yang, H., Liu, G., Liu, X., and Liu, J. (2017) Smart Cu(II)-aptamer complexes based gold nanoplatform for tumor micro-environment triggered programmable intracellular prodrug release, photodynamic treatment and aggregation induced photothermal therapy of hepatocellular carcinoma. *Theranostics 7*, 164–179.
(55) Lai, Z., Tan, J., Wan, R., Tan, J., Zhang, Z., Hu, Z., Li, J., Yang, W., Wang, Y., Jiang, Y., He, H., Yang, N., Lu, X., and Zhao, Y. (2017) An "activatable" aptamer-based fluorescence probe for the detection of HepG2 cells. *Oncol. Rep. 37*, 2688–2694.
(56) Deng, R., Qu, H., Liang, L., Zhang, J., Zhang, B., Huang, D., Xu, S., Liang, C., and Xu, W. (2017) Tracing the Therapeutic Process of Targeted Aptamer/Drug Conjugate on Cancer Cells by Surface-Enhanced Raman Scattering Spectroscopy. *Anal. Chem. 89*, 2844–2851.
(57) Hu, Z., Tan, J., Lai, Z., Zheng, R., Zhong, J., Wang, Y., Li, X., Yang, N., Li, J., Yang, W., Huang, Y., Zhao, Y., and Lu, X. (2017) Aptamer Combined with Fluorescent Silica Nanoparticles for Detection of Hepatoma Cells. *Nanoscale Res. Lett. 12*, 96.
(58) Berezovski, M. V, Lechmann, M., Musheev, M. U., Mak, T. W., and Krylov, S. N. (2008) Aptamer-facilitated biomarker discovery (AptaBiD). *J. Am. Chem. Soc. 130*, 9137–43.

(59) Kim, J. W., Kim, E. Y., Kim, S. Y., Byun, S. K., Lee, D., Oh, K.-J., Kim, W. K., Han, B. S., Chi, S.-W., Lee, S. C., and Bae, K.-H. (2014) Identification of DNA aptamers toward epithelial cell adhesion molecule via cell-SELEX. *Mol. Cells 37*, 742–746.
(60) Kim, K., Lee, S., Ryu, S., and Han, D. (2014) Efficient isolation and elution of cellular proteins using aptamer-mediated protein precipitation assay. *Biochem. Biophys. Res. Commun. 448*, 114–119.
(61) Van Simaeys, D., Turek, D., Champanhac, C., Vaizer, J., Sefah, K., Zhen, J., Sutphen, R., and Tan, W. (2014) Identification of cell membrane protein stress-induced phosphoprotein 1 as a potential ovarian cancer biomarker using aptamers selected by cell systematic evolution of ligands by exponential enrichment. *Anal. Chem. 86*, 4521–4527.
(62) Jia, W., Ren, C., Wang, L., Zhu, B., Jia, W., Gao, M., Zeng, F., Zeng, L., Xia, X., Zhang, X., Fu, T., Li, S., Du, C., Jiang, X., Chen, Y., Tan, W., Zhao, Z., and Liu, W. (2016) CD109 is identified as a potential nasopharyngeal carcinoma biomarker using aptamer selected by cell-SELEX. *Oncotarget 7*, 55328–55342.
(63) Ara, M. N., Hyodo, M., Ohga, N., Akiyama, K., Hida, K., Hida, Y., Shinohara, N., and Harashima, H. (2014) Identification and expression of troponin T, a new marker on the surface of cultured tumor endothelial cells by aptamer ligand. *Cancer Med. 3*, 825–834.
(64) Sobczyk, G. J., Wang, J., and Weijer, C. J. (2014) SILAC-based proteomic quantification of chemoattractant-induced cytoskeleton dynamics on a second to minute timescale. *Nat. Commun. 5*, 1–14.
(65) Dua, P., Kim, S., and Lee, D. (2011) Nucleic acid aptamers targeting cell-surface proteins. *Methods 54*, 215–225.
(66) Rybak, J. N., Scheurer, S. B., Neri, D., and Elia, G. (2004) Purification of biotinylated proteins on streptavidin resin: A protocol for quantitative elution. *Proteomics 4*, 2296–2299.
(67) Betancourt, T., Brown, B., and Brannon-Peppas, L. (2007) Doxorubicin-loaded PLGA nanoparticles by nanoprecipitation: preparation, characterization and in vitro evaluation. *Nanomedicine (London, U. K.) 2*, 219–32.
(68) Betancourt, T., Byrne, J. D., Sunaryo, N., Crowder, S. W., Kadapakkam, M., Patel, S., Casciato, S., and Brannon-Peppas, L. (2009) PEGylation strategies for active targeting of PLA/PLGA nanoparticles. *J. Biomed. Mater. Res., Part A 91*, 263–276.
(69) Dyballa, N., and Metzger, S. (2012) Fast and sensitive coomassie staining in quantitative proteomics, in *Quantitative Methods in Proteomics*, pp 47–59.
(70) Zuker, M. (2003) Mfold web server for nucleic acid folding and hybridization prediction. *Nucleic Acids Res. 31*, 3406–3415.
(71) Bailly-Maitre, B., de Sousa, G., Boulukos, K., Gugenheim, J., and Rahmani, R. (2001) Dexamethasone inhibits spontaneous apoptosis in primary cultures of human and rat hepatocytes via Bcl-2 and Bcl-xL induction. *Cell Death Differ. 8*, 279–288.
(72) Tacar, O., Sriamornsak, P., and Dass, C. R. (2013) Doxorubicin: An update on anticancer molecular action, toxicity and novel drug delivery systems. *J. Pharm. Pharmacol. 65*, 157–170.

(73) Wang, J., Ma, L., Tang, X., Zhang, X., Qiao, Y., Shi, Y., Xu, Y., Wang, Z., Yu, Y., and Sun, F. (2015) Doxorubicin induces apoptosis by targeting Madcam1 and AKT and inhibiting protein translation initiation in hepatocellular carcinoma cells. *Oncotarget 6*, 24075–91.
(74) Jin, C., Qiu, L., Li, J., Fu, T., Zhang, X., and Tan, W. (2016) Cancer biomarker discovery using DNA aptamers. *Analyst 141*, 461–466.
(75) Conrads, T. P., Issaq, H. J., and Hoang, V. M. (2003) Current Strategies For Quantitative Proteomics, in *Proteome Characterization and Proteomics*, pp 133–159. Elsevier Inc.
(76) Pang, Z., Al-Mahrouki, A., Berezovski, M., and Krylov, S. N. (2006) Selection of surfactants for cell lysis in chemical cytometry to study protein-DNA interactions. *Electrophoresis 27*, 1489–1494.
(77) Hollinshead, M., Sanderson, J., and Vaux, D. J. (1997) Anti-biotin Antibodies Offer Superior Organelle-specific Labeling of Mitochondria over Avidin or Streptavidin. *J. Histochem. Cytochem. 45*, 1053–1057.
(78) Niers, J. M., Chen, J. W., Weissleder, R., and Tannous, B. A. (2011) Enhanced in vivo imaging of metabolically biotinylated cell surface reporters. *Anal. Chem. 83*, 994–999.
(79) Alon, R., Bayer, E. A., and Wilchek, M. (1990) Streptavidin contains an RYD sequence which mimics the RGD receptor domain of fibronectin. *Biochem. Biophys. Res. Commun. 170*, 1236–1241.
(80) Singer, I. I., Kawka, D. W., Kazazis, D. M., and Clark, R. A. F. (1984) In vivo co-distribution of fibronectin and actin fibers in granulation tissue: Immunofluorescence and electron microscope studies of the fibronexus at the myofibroblast surface. *J. Cell Biol. 98*, 2091–2106.
(81) Klockenbusch, C., and Kast, J. (2010) Optimization of Formaldehyde Cross-Linking for Protein Interaction Analysis of Non-Tagged Integrin β1. *J. Biomed. Biotechnol. 2010*, Article ID 927585.